

Ice Nucleating Particles Variability Across a Megacity

Sebastián Mendoza-Téllez¹, Karla Valdés², David Ramírez², Jan Alexis Cedillo³, Olivia Rivera-Hernández⁴, Fernanda Córdoba¹, Harry Alvarez⁵, Javier Miranda⁶, Irma Rosas¹, Graciela B. Raga¹, Emma Negrete¹, Leticia Martínez¹, Eva Salinas¹, and Luis A. Ladino^{1,*}

¹Institute for Atmospheric Sciences and Climate Change, Universidad Nacional Autónoma de México, Mexico City, Mexico

²División de Ciencias Biológicas y de la Salud, Universidad Autónoma Metropolitana – Xochimilco, Mexico City, Mexico

³Escuela Nacional de Ciencias Biológicas, Instituto Politécnico Nacional, Mexico City, Mexico

⁴Dirección de Monitoreo de Calidad del Aire, Secretaría del Medio Ambiente, Ciudad de México, Mexico

⁵Facultad de Ciencias, Universidad Nacional Autónoma de México, Mexico City, Mexico

⁶Instituto de Física, Universidad Nacional Autónoma de México, Mexico City, Mexico

*Corresponding author: Luis A. Ladino (luis.ladino@atmosfera.unam.mx)

Abstract

Megacities are a ~~great~~-major source of urban aerosol particles, which can impact cloud formation and the local hydrological cycle. However, the aerosol-cloud interaction ~~in~~-above megacities, especially in their different microclimates, is poorly understood. In the present study, the physicochemical and biological properties of urban aerosol particles, along with their ice nucleating particle (INP) concentration via immersion freezing and as a function of particle size (0.56 μm to 10 μm), were simultaneously characterized at two sites across the Mexico City Metropolitan Area (MCMA). We found differences in the chemical composition, criteria pollutants ($\text{PM}_{2.5}$, O_3 , CO , NO_x , and SO_2), and biological content between northern and southern MCMA, separated by 16 km. The collected urban MCMA aerosol particles were found to act as INPs, with average concentrations ranging between $0.04 \pm 0.04 \text{ L}^{-1}$ (at -15°C) and $24.9 \pm 18 \text{ L}^{-1}$ (at -30°C). Although the measured INP concentrations were similar in both sites, the southern samples showed a higher INP concentration for larger aerosol particles (i.e., particles between 5.6-10 μm).

Although the urban aerosol's physicochemical properties, biological content, and its sources were found to differ at both sites, it did not strongly impact the INP concentrations, with the exception of the largest measured particles. This highlights the importance of considering that aerosol-cloud interactions ~~within~~-above a megacity may vary, especially when assessing the role of INPs in cloud formation.

41 **1. Introduction**

42 Mexico City and its Metropolitan Area (MCMA) is one of the top megacities worldwide with
43 a population of 21 million inhabitants (Población, 2025). In the 1980s, the MCMA was reported
44 as the most polluted city on Earth (Molina and Molina, 2004); however, since the 1990s, air
45 quality has improved significantly (Lezama and Vargas, 2000). Even so, due to its size and the
46 diverse anthropogenic activities, the MCMA atmospheric processes are complex and far from
47 being completely understood (Molina et al., 2010). Nowadays, poor air quality is one of the
48 major threats for the MCMA inhabitants' health (Riojas-Rodríguez et al., 2014). The impact of
49 the high annual release of particulate matter (PM) (in the order of gigagrams, Gg) on the local
50 climate remains poorly quantified (Castro Romero et al., 2024).

51
52 Several studies have provided substantial insights into the physicochemical properties of PM
53 within the MCMA (Aldape et al., 1991; Edgerton et al., 1999; Doran et al., 2007; Querol et al.,
54 2008). For example, Vega et al. (2004) characterized the PM_{2.5} composition of the MCMA,
55 showing that the sulfate (SO₄²⁻), ammonium (NH₄⁺), and total carbon (elemental carbon +
56 organic carbon) average concentrations are higher in the north of the city compared to the
57 southern part (higher by 1.16 µg m⁻³ (18.1 %), 0.8 µg m⁻³ (23.6 %), and 18.49 µg m⁻³ (51.1 %),
58 respectively). This agrees with the data reported by the 2006 MILAGRO (Megacity Initiative:
59 Local And Global Research Observations) project, where a complete evaluation of the regional
60 and global impacts of Mexico's City atmospheric emissions was assessed (Molina et al., 2010).

61
62 Several studies found that organic matter has a huge impact on the MCMA's PM_{2.5}
63 composition. Amador-Muñoz et al. (2011) reported a carbon preference index (CPI) larger than
64 1 on the southwest of the MCMA, suggesting that this part of the city contains more biogenic
65 sources (Amador-Muñoz et al., 2013). Ladino et al. (2018) and Hernández-López et al. (2023)
66 reported clear differences in polycyclic aromatic hydrocarbons (PAHs) between the north and
67 south of the MCMA, with the highest concentrations reported in the northern part of the city.
68 Gasoline-fueled vehicles are likely responsible for local PAHs emissions and could reinforce
69 the presence of urban microclimates with independent local atmospheric processes, inside one
70 megacity (Molina and Molina, 2004).

71
72 A microclimate can be referred to as a relative small-scale area with a distinctive climate over
73 it as a whole (Met Office Factsheet 14). ~~Thanks~~Owing to its large area, and the clear variability
74 of land use (e.g., industrial, rural, residential, commerce, and ecological preservation), the

75 northern and southern MCMA present significant differences in temperature (heat islands),
76 rainfall, wind patterns, humidity, aerosol and gas emissions, indicating the presence of a clear
77 microclimate differentiation (Met Office Factsheet 14; Molina and Molina, 2004; Amador-
78 Muñoz et al., 2013; Castro Romero et al., 2024). Although the studies above highlight the clear
79 differences in the sources and physicochemical properties of PM in different parts of the
80 MCMA, studies that include simultaneous measurements at two or more sites are scarce. This
81 is of high importance to understand the microclimates along the MCMA and their relationship
82 with local precipitation events. Zhu et al. (2024) evaluated precipitation events across China,
83 finding that precipitation characteristics could differ across climatic zones. Additionally, Li et
84 al. (2019) showed that atmospheric circulation changes driven by global warming modulated
85 the intensification of extreme precipitation events across North America.

86

87 Meteorological data and models indicate a predominance of northerly, southerly, southwesterly,
88 and northeasterly wind events in MCMA, with frequencies of 20 %, 16 %, 15 %, and 13 %,
89 respectively (Celada-Murillo et al., 2013). In addition, typically wind events with speeds
90 ranging from 0.25 to 1.50 m s⁻¹ appear mainly during the early morning, while other wind events
91 with larger speeds (i.e., ranging from 1.5 to 5.50 m s) appear mainly during the afternoon and
92 night (Celada-Murillo et al., 2013; Salcido et al., 2015). On the other hand, meteorological
93 conditions in some defined area, as the presence of atmospheric stable conditions, or the well-
94 known large-scale atmospheric circulation could help understanding the real perturbations of
95 urban aerosols on cloud formation and precipitation events (Trofimov et al., 2022).

96

97 Given that most of the precipitation over the tropics comes from ice-containing clouds
98 (Mülmenstädt et al., 2015) and that aerosol particles acting as ice nucleating particles (INPs)
99 are key in mixed-phase cloud (MPC) formation (Rogers and Yau, 1996; Houze, 2014; Kanji et
100 al., 2017), information on the interplay between aerosol particles and cloud formation in big
101 cities such as the MCMA is urgently needed, especially because extreme precipitation events
102 are predicted to increase with time (Tabari, 2020; Gimeno et al., 2022), causing huge
103 economical and societal impacts in densely populated cities. Aerosol particles have the potential
104 to influence the development of deep convective clouds ~~those of,~~ which are typically associated
105 with extreme rainfall events (Burrows et al., 2022). Efficient INPs can promote specific
106 processes as the seeder-feeder mechanism (Ohneiser et al., 2025) triggering primary ice particle
107 formation as well as ice multiplication, increasing the ice water content in MPC (Purdy et al.,
108 2005). These ice particles can grow at expenses of the surrounding water droplets, via the

109 Wegner-Bergeron-Findeisen process, enhancing precipitation rates (Heymsfield et al., 2020;
110 Ohneiser et al., 2025). Toll et al. (2024) showed that the presence of anthropogenic particles
111 hot spots can modify cloud microphysics, leading to cloud glaciation and precipitation events
112 under stratiform non-convective clouds.

113

114 The impact of urban particles on ice formation in MPCs is well documented (e.g., Hasenkopf
115 et al., 2016; Pereira et al., 2021; Chen et al., 2024). For example, Zhao et al. (2019) reported
116 that the presence of urban aerosol particles affects the microphysical properties of clouds under
117 moderate convective conditions, decreasing ice crystal number concentration (ICNC) and thus
118 increasing the ice particle effective radius (R_{ei}). Chen et al. (2024) found that urban super-
119 micron traffic-influenced road dust and construction-related dust particles were the primary
120 source of INPs (heat-resistant INPs) at temperatures below $-15\text{ }^{\circ}\text{C}$ in Beijing, China.
121 Nevertheless, given that urban aerosol particles are a complex multicomponent mixture (i.e.,
122 biological, dust, black carbon, and biomass burning (BB) particles, among others), they may
123 contain components with contrasting ice nucleation abilities. Although urban centers clearly
124 experience high aerosol concentrations, INP concentrations in megacities do not necessarily
125 increase during heavily polluted periods (e.g., Bi et al., 2019; Cabrera-Segoviano et al., 2022;
126 Chen et al., 2024).

127

128 The role of urban particles emitted in the MCMA in ice-cloud formation has been previously
129 evaluated (Knopf et al., 2010; Pereira et al., 2021; Rodríguez-Gómez, 2021; Cabrera-Segoviano
130 et al., 2022; Melchum et al., 2023). The first ice nucleation study in the MCMA was conducted
131 by Knopf et al. (2010) as part of the MILAGRO project. The authors reported that the particles
132 in the northern part of the City are dominated by organics, and can efficiently act as INP under
133 cirrus and MPC conditions, i.e., relative humidity with respect to ice (RH_{ice}) of $\sim 105\%$ to 150%
134 and temperatures of 205 K to 255 K .

135

136 Regarding MPC, Pereira et al. (2021) found that the ubiquitous anthropogenic emissions did
137 not have a significant impact on the INP concentrations, with samples collected in rural and
138 urban sites, both in the south of the MCMA. Cabrera-Segoviano et al. (2022) reported an inter-
139 annual variability of INP concentrations (a one order of magnitude difference at temperatures
140 higher than $-20\text{ }^{\circ}\text{C}$) at southern MCMA between 2018 and 2019, a fact that can be related to the
141 variability in aerosol emissions like re-suspended dust. Rodríguez-Gómez (2021) reported
142 higher INP concentrations in the planetary boundary layer compared to the free troposphere on

143 samples collected in southern MCMA during the BB season, similar to previous studies (Prenni
144 et al., 2012; Jahn et al., 2020; Jahl et al., 2021). Finally, Melchum et al. (2023) evaluated the
145 INP abilities of different airborne microorganisms from tropical places such as MCMA and other
146 sites ~~along~~ across Mexico. The authors found that out of the 64 tested microorganisms, only the
147 *Cupriavidus pauculus* (proteobacteria) and the *Phaeocystis* sp. (marine phytoplankton) can be
148 relevant to MPC formation (with onset freezing temperatures, T_0 of -11.8 °C and -16.0 °C,
149 respectively).

150

151 Although PM and INPs have been previously characterized in the MCMA, simultaneous INP
152 measurements at more than one site have never been reported. Therefore, there is a poor
153 understanding of how urban aerosol particles could influence cloud formation across the
154 different MCMA's microclimates. To fill this gap in knowledge, the present study reports the
155 simultaneous characterization (physical, chemical, and biological) of PM_{2.5} as well as the INP
156 concentration in a northern and a southern site within the MCMA. To the best of our knowledge,
157 this is the first time that such comprehensive evaluation of the aerosol-cloud interactions is
158 performed in this megacity.

159

160 **2. Methods**

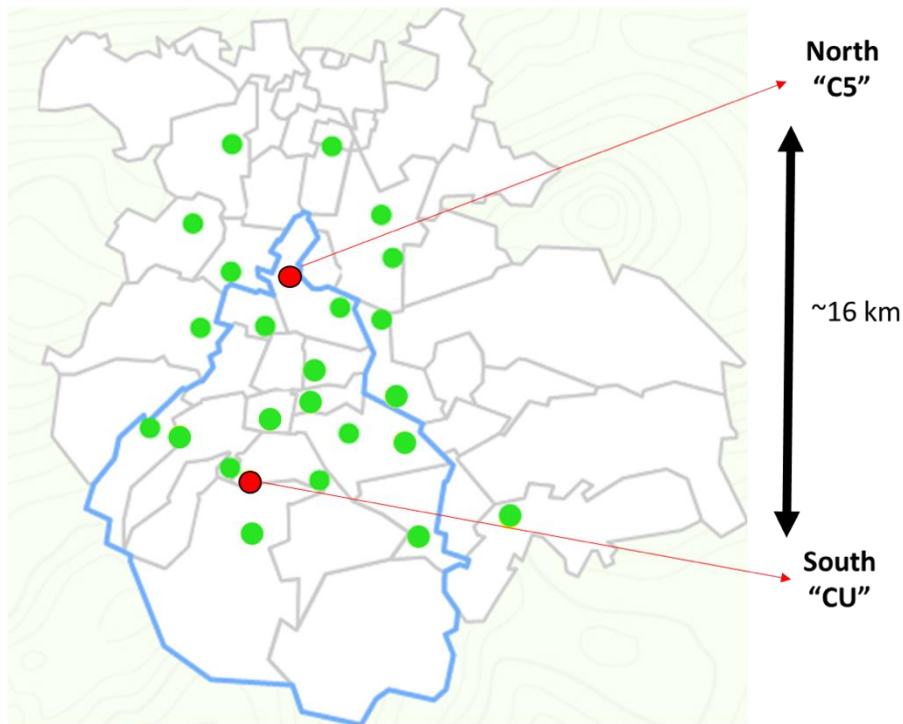
161 **2.1 Sampling location**

162 Mexico City is a tropical city located at 2240 m a.s.l. (Población, 2025), with a particular
163 topography that influences the accumulation of air pollutants (Molina and Molina, 2004). With
164 a sub-humid climate, the city presents an average annual temperature (between 1950 and 2013)
165 of 15 to 18 °C (Behzadi et al., 2020). The MCMA experiences three different seasons such as
166 cold-dry: October-February, warm-dry: March-May, and wet season: June-October. The mean
167 annual precipitation within 1950–2013 for Mexico City was reported to vary between 357 mm
168 year⁻¹ and 1298 mm year⁻¹ (Jáuregui, 2000; Molina et al., 2009; Behzadi et al., 2020; Cabrera-
169 Segoviano et al., 2022).

170

171 A short-term field campaign was carried out simultaneously at the north and south of the
172 MCMA during the dry-warm season, i.e., between May 12th and May 20th, 2022. Both
173 sampling sites are located within Mexico City (Fig. 1), and they are ~16 km away from each
174 other.

175



176

177 Figure 1. Location of the MCMA showing Mexico City (blue contour) as well as northern and
 178 southern sampling sites (red circles). The green circles represent the Mexico City atmospheric
 179 monitoring stations. Modified from <https://aire.cdmx.gob.mx/>

180

181 Sampling at the southern site (CU, 19.3262° N 99.1761° W) took place on the roof of the
 182 Institute for Atmospheric Sciences and Climate Change building (approx. 15 m a.g.l.), on the
 183 main campus of the Universidad Nacional Autónoma de México (UNAM). Traffic is the
 184 primary source of anthropogenic pollution at this site. However, an ecological reserve (237 ha)
 185 is located within the main UNAM campus, with the vegetation being dry and brown and
 186 susceptible to forest fires during the sampling period. It can provide biological material to the
 187 atmosphere through the native and introduced species of plants, animals, and microorganisms
 188 that live in it (Melchum et al., 2023).

189

190 On the other hand, the sampling at the northern site (C5, 19.483781° N 99.147312° W) took
 191 place on the roof of the Environmental Analysis Laboratory (C5) building (approx. 5 m a.g.l.)
 192 of the Mexico City Atmospheric Monitoring System (<http://www.aire.cdmx.gob.mx/>). The C5
 193 sampling site is subject to a wide range of anthropogenic sources, as it is located in the city's
 194 popularly known “industrial area.” Traffic, industrial, and other anthropogenic emissions
 195 contribute to high PM atmospheric concentrations at this sampling site (Castro Romero et al.,
 196 2024).

197
198
199
200
201
202
203
204
205
206
207

Meteorological (T, RH, wind direction, wind speed, solar radiation, and precipitation) and criteria pollutants (PM_{2.5}, O₃, CO, NO_x, and SO₂) data were recorded on both sites during the sampling campaign (Tables S1 and S2, and Figs. S1 and S2). The campaign dates, total sampling times and volumes are shown in Table 1. The ionic composition and elemental composition were obtained using ion chromatography and X-ray fluorescence, respectively, on the 24-hour collected samples. Culturable microorganisms were obtained through different microbiological analysis described in section 2.2.5, on 5 min collected samples. ~~All sampling was performed on May 12th, May 13th, May 16th, May 17th, May 18th, May 19th and May 20th, 2022.~~

208 Table 1. Sampling campaign description: dates, total sampling times, and sampling volume are
209 shown for the three sampling methods: MiniVol (2.5 µm cut-off) for chemical analysis,
210 MOUDI (0.56 to 10 µm cut-off, see section 2.2.6) for INP analysis, and BioStage (10 µm cut-
211 off) for biological analysis. Note that the sampling times were the same at both sites.

SAMPLING CAMPAIGN								
Date (month- day- year)	MiniVol ¹ (chemical analysis)		MOUDI ² (INP analysis)				BioStage ³ (biological analysis)	
	Total sampling time (h)	Sampling volume (m ³)	Initial sampling time (local time, h)	Final sampling time (local time, h)	Total sampling time (h)	Sampling volume (m ³)	Total sampling time (h)	Sampling volume (m ³)
05-12-22	24	7.2	-	-	-	-	0.08	0.1
05-13-22	24	7.2	-	-	-	-	0.08	0.1
05-14-22	24	7.2	-	-	-	-	0.08	0.1
05-15-22	24	7.2	-	-	-	-	0.08	0.1
05-16-22	24	7.2	8:37	12:58	4:21	7.8	0.08	0.1
05-17-22	24	7.2	8:20	12:20	4:00	7.2	0.08	0.1
05-18-22	24	7.2	8:04	12:06	4:02	7.3	0.08	0.1
05-19-22	24	7.2	8:44	12:56	4:12	7.6	0.08	0.1
05-20-22	24	7.2	8:43	12:50	4:07	7.4	0.08	0.1

212 **Flow rates: ¹ 15 L/min, ² 30 L/min, ³ 28.3 L/min**

213

214 **2.2 Sampling and instrumentation**

215 The simultaneous sampling was performed using, per site, a MiniVol TAS (Tactical Air
216 Sampler; Airmetrics) with a 2.5 µm cut-size inlet operated at 5 L min⁻¹, an eight stage micro-

217 orifice uniform deposit impactor (MOUDI 100R; MSP) operated at a 30 L min⁻¹ flow rate to
218 separate particles as a function of their aerodynamic diameter (cut sizes of 0.18 µm, 0.32 µm,
219 0.56 µm, 1.0 µm, 1.8 µm, 3.2 µm, 5.6 µm and 10 µm), and a single-stage BioStage Quick Take
220 30 cascade impactor for viable particles (SKC Inc. USA) operated at a 28.3 L min⁻¹ flow rate.
221 The MOUDI samples, used to evaluate the INP concentrations, were collected one time a day
222 from May 16th to May 20th, 2022, with the sampling times shown in Table 1 (more details are
223 provided in section 2.2.6). The MiniVol samples were collected daily for 24 h on May 12th,
224 May 13th, May 16th, May 17th, May 18th, May 19th and May 20th, 2022, on 47 mm Teflon filters
225 (Pall Science), and were used for the ionic and elemental composition analysis. The BioStage
226 impactor samples with a 10 µm cut-size inlet were used for culturable bacteria and fungi
227 identification. They were collected once a day (at 10:00 am for 5 mins) on the same dates as
228 the MiniVol samples (more details are described in section 2.2.5). The general [description](#)
229 [overview](#) of the sampling campaign is shown in Table 1.

230

231 **2.2.1 Meteorological data**

232 Meteorological variables such as temperature, relative humidity, wind direction, wind speed,
233 and solar radiation were obtained from the meteorological stations (Campbell Scientific) of the
234 Red Universitaria de Observatorios Atmosféricos (RUOA) and the Programa de Estaciones
235 Meteorológicas del Bachillerato Universitario (PEMBU) placed in CU and C5, respectively.
236 Also, back trajectories of the air masses arriving in both sampling sites were obtained using the
237 Hybrid Single-Particle Lagrangian Integrated Trajectory (HYSPLIT) model from the National
238 Oceanic and Atmospheric Administration (NOAA) for 72 h at 250 m a.g.l (Draxler, 2010).

239

240 **2.2.2 Criteria pollutants**

241 The concentrations of O₃, CO, NO_x, and SO₂, were measured with the Teledyne (Sandiego,
242 CA) ultraviolet photometry API Model 400E non-dispersive infrared analyzer, API model
243 300E, and API model 200E, respectively. The PM_{2.5} was measured with a Thermo Scientific
244 (Franklin, MA) tapered element oscillating microbalance (TEOM) Model 1400A ambient
245 particulate monitor at a flow rate of 3 L min⁻¹.

246

247 **2.2.3 PM_{2.5} ionic composition**

248 The ionic composition was obtained using a Dionex ICS-1500 ion chromatography (IC) at the
249 Laboratorio de Aerosoles Atmosféricos of the Institute for Atmospheric Sciences and Climate
250 Change, UNAM. For PM_{2.5} aerosol sample extraction, the MiniVol sample filters (i.e., 47 mm

251 Teflon filters) were submerged in 10 mL of deionized water, sonicated for one hour (using an
252 ultrasonic bath at a temperature below 27 °C), and shaken at 350 rpm for six hours (Sartorius
253 CPA225D).

254

255 Anion analysis was performed using a Dionex IonPac AS23 column (4 × 250 mm) and a
256 carbonate solution (Na₂CO₃ 4.5 mM – NaHCO₃ 0.8 mM) as the mobile phase at a flow rate of
257 1 mL min⁻¹. Three anions (i.e., NO₃³⁻, SO₄²⁻, and Cl⁻) were measured using the described setup.
258 Cation analysis was performed using a Dionex IonPac CS12A column (4 mm × 250 mm) and
259 a methanesulfonic acid (CH₄O₃S 20 mM) with a flow rate of 1 mL min⁻¹ as a mobile phase.
260 Five cations (i.e., Na⁺, K⁺, NH₄⁴⁺, and Ca²⁺) were measured using the described setup. The limits
261 of quantification (LOQ) and determination (LOD) were calculated using the linear regression
262 of standards calibration. More details about IC setup and similar methods can be found in Castro
263 Romero et al. (2024).

264

265 **2.2.4 PM_{2.5} X-ray fluorescence**

266 The elemental composition analysis was performed at the Laboratorio de Aerosoles, Instituto
267 de Física, UNAM following Espinosa et al. (2012). An X-ray fluorescence spectrometer with
268 an Oxford Instruments (Scotts Valley, CA, USA) tube with Rh anode and an Amptek X-
269 123SDD spectrometer (Bedford, MA, USA) was used to obtain the elemental composition of
270 all MiniVol ~~particle-sample~~ filters (i.e., 47 mm Teflon filters)s. The instrument was operated at
271 50 kV and a current of 750 μA, irradiating for 900 s per spectrum. More details of instrument
272 calibration can be found at Espinosa et al. (2012). The chemical composition was quantified
273 using the methodology reported by Espinosa et al. (2010). The percentage fraction for each
274 element was determined by using the relationship between the analyzed element concentration
275 and the total mass concentration.

276

277 **2.2.5 Airborne culturable microorganisms' collection and identification**

278 For the microorganism's identification (bacteria and fungi), petri dishes (100 mm × 10 mm)
279 with three different media were used to impact and collect particles of 10 μm or less in size,
280 and grow the microorganisms using the BioStage impactor: trypto-casein soy agar (TSA, BD,
281 Bioxon) supplemented with 100 mg L⁻¹ of cycloheximide (Sigma-Aldrich) (to prevent growth
282 fungal propagules) for mesophilic cultivable bacteria (MCB), Reasoner's 2A (R2A, Condalab)
283 for slow-growing species of MCB, and malt extract agar (MEA, BD Bioxon) for cultivable
284 fungal propagules. The sampling time on the BioStage impactor was set to 5 min.

285

286 The concentrations of cultivable bacteria were reported as Colony Forming Units per m³ of air
287 (CFU m⁻³). The following procedure was applied as described in Melchum et al. (2023). The
288 TSA, R2A, and MEA were cultured at 35 °C, 35 °C, and 25 °C, respectively. After 48 h (for
289 TSA bacteria) and 72 h (for R2A bacteria and fungi), the CFU were quantified, and the Petri
290 dishes were sealed with parafilm and stored at 4 °C for further analysis. Representative bacterial
291 colonies were randomly selected and purified by several reseedings in TSA. Gram staining was
292 performed to classify the bacteria as Gram-positive or Gram-negative by microscopic
293 observation (100×) of the preparations. Isolated bacteria confirmation of identity was
294 performed by mass spectroscopy, using the Microflex MALDI-TOF MS® (Bruker Daltonics,
295 Bremen, Germany). The identification of fungal species was carried out at the genus level using
296 taxonomic keys based on macroscopic colony characteristics and spore microscopic
297 examination (60×) (Rodriguez-Gomez et al., 2020; Melchum et al., 2023).

298

299 **2.2.6 Ice nucleation experiments**

300 The INP concentration of the collected aerosol particles were obtained using a UNAM-Micro-
301 orifice Uniform Deposit Impactor-Droplet Freezing Technique (UNAM-MOUDI-DFT),
302 described in Córdoba et al. (2021) with its main features shown in Fig. S3.

303

304 Aerosol particles were collected on hydrophobic glass coverslips as substrates at 0.56 µm, 1.0
305 µm, 1.8 µm, 3.2 µm, 5.6 µm and 10 µm cut-offs MOUDI stages (flow rate of 30.0 L min⁻¹).
306 After sampling, every substrate was stored in sealed, sterilized Petri dishes at 4 °C until its
307 analysis.

308

309 Each glass coverslip was analyzed using the UNAM-MOUDI-DFT to simulate the immersion
310 freezing mode between 0 °C and -40 °C. For the INP experiments, the glass coverslips were
311 placed on a sample holder inside the cold cell with the sample holder at the top of two blocks
312 for a sample temperature control: a heating block (copper-made block with two heating
313 resistances, 100 W and 120 V) and a cooling block (cooled by refrigerator circulator, PRO-
314 RP1090, LAUDA), with the cold block at the bottom. To induce droplet formation, humid air,
315 carried by nitrogen (grade 4.8, INFRA), is directed toward the sample holder at 0 °C. Once
316 approx. 30-40 droplets of ca. 170 µm radius are formed, ~~and~~ a dry airstream is introduced into
317 the cold cell to shrink the droplets, aiming to minimize contact between them. Finally, the cold
318 cell was isolated, and a temperature ramp from 0 °C to -40 °C (at a cooling rate of 10 °C min⁻¹

319 ¹) was run until the freezing of each drop was observed. The entire process was recorded with
320 a video camera (MC500-W, JVLAB) attached to an optical microscope (Axiolab Zeiss,
321 Germany) with a 5×/0.12 magnification objective, the microscope objective being coupled to
322 the sample holder via a glass coverslip at the top of the cold cell.

323

324 From the recorded video, it is possible to determine the freezing temperature for each droplet,
325 which allows calculation of the frozen fraction (F_{ice}) and the INP number concentration as a
326 function of temperature ([INP(T)]). F_{ice} was calculated using Equation 1:

$$327 \quad F_{ice} = \frac{N_{ice}}{N_{ice} + N_{droplets}} \quad (1)$$

328 where N_{ice} and $N_{droplets}$ are the number of frozen droplets (dimensionless) and the number of
329 unfrozen droplets (dimensionless), respectively (Kanji et al., 2017).

330

331 The [INP(T)] was calculated using Equation 2 (Mason et al., 2015; Córdoba et al., 2021):

332

$$333 \quad [INP(T)] = -\ln\left(\frac{N_u(T)}{N_0}\right) \cdot \left(\frac{A_{deposit}}{A_{DFT}V}\right) \cdot N_0 \cdot f_{ne} \cdot f_{nu,0.25-0.10\text{ mm}} \cdot f_{nu,1\text{ mm}} \quad (2)$$

334

335 where $N_u(T)$ is the number of unfrozen droplets at T (°C), N_0 is the total number of droplets
336 (dimensionless), $A_{deposit}$ is the total area of the aerosol particles deposited on the hydrophobic
337 glass coverslip (cm²), A_{DFT} is the area of the sample analyzed by the DFT (cm²), V is the volume
338 of air through the MOUDI (L), f_{ne} is a correction factor to account for the uncertainty associated
339 with the number of nucleation events in each experiment (dimensionless), and f_{nu} is a correction
340 factor to account for changes in particle concentration across each MOUDI sample
341 (dimensionless). Additionally, this equation accounts for the possibility that multiple particles
342 may be present within a droplet (Vali, 1996), the correction for the total area covered by
343 particles deposited on the MOUDI coverslips, and corrections for inhomogeneities in particle
344 deposition. More details of Equation 2 and the applied corrections can be found in Mason et al.
345 (2015).

346

347 **2.2.7 Data analysis**

348 The STATISTICA[®] 12 software (StatSoft, TIBCO Software Inc., USA) was employed to
349 evaluate basic statistics and cluster analysis of data from the different analysis described in
350 section 2.2. With the main objective of identifying associations among chemical species and

351 their possible sources, a cluster analysis using Ward's method of amalgamation and Pearson
352 correlation coefficients was carried out to construct dendrograms for both sampling sites.

353

354 3. Results and Discussion

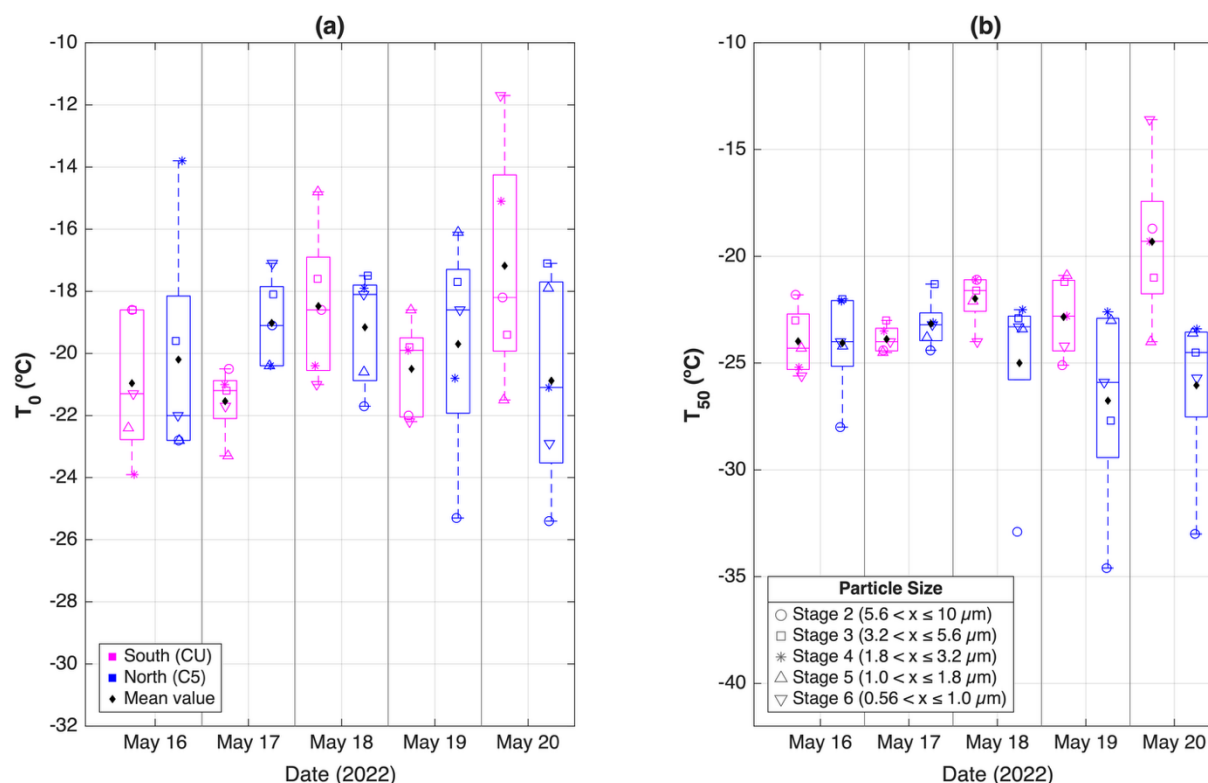
355 3.1 Frozen fraction and INP concentration variability

356 Following the procedure described in section 2.2.6, the frozen fraction and the INP
357 concentrations were obtained for each sample from May 16th to 20th. Figure S4 shows the frozen
358 fraction (FF) as a function of particle size (aerodynamic diameters of 0.56 μm to 10 μm) for
359 the northern and the southern sampling sites. This size range was selected considering that
360 super-micron particles contribute more than 70 % to the total INP population (e.g., Mason et
361 al., 2016; Córdoba et al., 2021). Aerosol particles collected in the present study were able to
362 nucleate ice at temperatures warmer than those required to freeze supercooled liquid drops (i.e.,
363 homogeneous freezing, black line). The homogeneous freezing line was determined using the
364 same procedure described in section 2.2.6 with a brand-new substrate (i.e., without aerosol
365 particles impacted on them). The ~~average onset freezing temperature (T_0)FF curve~~ of the
366 homogeneous freezing experiments (~~i.e., -34.28 °C~~) is comparable with other data for
367 supercooled liquid drops such as the 100 μm (~~-34.15 °C~~) and 89 ± 7 μm (~~-35.5 to -36.7 °C~~)
368 liquid water drops reported by Shardt et al. (2022) and Tarn et al. (2021), respectively.

369

370 ~~For a more quantitative comparison of the ice nucleating abilities of northern and southern~~
371 ~~samples, the onset freezing temperatures (T_0) and the temperatures at which 50 % of the droplets~~
372 ~~freeze (T_{50}) for each sample were determined as shown in Fig. 2. Overall, the average T_0 and~~
373 ~~T_{50} values were similar between northern and southern MCMA samples. The highest average~~
374 ~~T_0 difference between the northern and southern samples was registered on May 20th (Fig. 2a),~~
375 ~~with T_0 values of (-20.9 ± 3.5) °C and (-17.2 ± 3.8) °C for C5 and CU, respectively. Additionally,~~
376 ~~the greatest distinction between northern and southern T_{50} values was again recorded on May~~
377 ~~20th, with $T_{50} = (-19.3 \pm 3.8)$ °C on CU, and $T_{50} = (-26.1 \pm 3.9)$ °C on C5. The warmest average~~
378 ~~T_0 value (-17.2 °C) reported in this work is slightly higher than those reported by Knopf et al.~~
379 ~~(2010) (-19.15 °C, warmer T_0 for immersion freezing mode), Rodríguez-Gómez (2021)~~
380 ~~(warmer $T_0 = -19.3$ °C), Cabrera-Segoviano et al. (2022) (warmer $T_0 = -20.3$ °C); and lower~~
381 ~~than the reported by Pereira et al. (2021) (warmer $T_0 = -7.5$ °C). Taking uncertainties into~~
382 ~~account, the T_0 values reported in this work partially differ from literature data for MCMA,~~

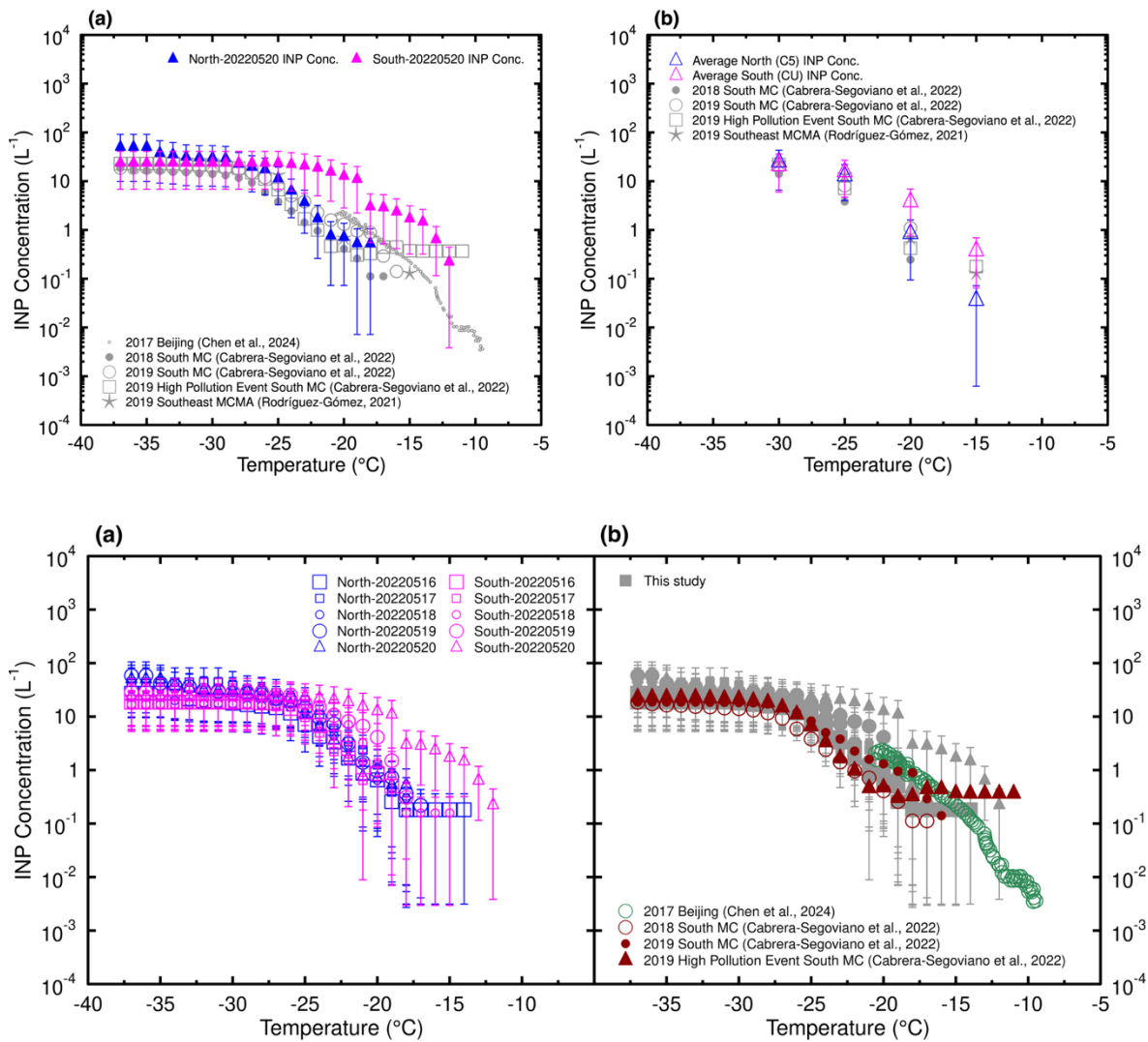
383 showing a variation that local emissions could influence each sampling point (e.g., Pereira et
 384 al. (2021) warmer T_0 was found at Altzomoni site, a semi-pristine area at MCMA southeast).



386
 387 **Figure 2.** Boxplots of (a) onset freezing temperatures (T_0) and (b) median freezing temperatures
 388 (T_{50}) for samples collected at the north (C5, blue) and south (CU, magenta) of Mexico City
 389 between May 16th and May 20th. The bottom and top limits of each box represent the 25th and
 390 75th percentiles, respectively. The horizontal line inside each box indicates the median
 391 temperature. The top and bottom whiskers show the minimum and maximum temperature
 392 values, respectively. Real values for each MOUDI stage, from 2 (larger aerodynamical size) to
 393 6 (smaller aerodynamical size), are represented by circles, squares, asterisks, upward triangles,
 394 and downward triangles, respectively. The black diamonds indicate the mean values for each
 395 data group.

396
 397 The total INP concentrations (i.e., the accumulated INP concentration, represented by the sum
 398 of each MOUDI stage INP concentration for each sample) at both sites are shown in Fig. 23a.
 399 Although the INP concentrations measured at both sites were comparable, the exemption was
 400 the May 20th sample (Fig. 23a), where higher and statistically significant differences in INP
 401 concentrations were measured in the southern site between -19 °C and -22 °C (considering the
 402 Agresti and Coull (1998) method to calculate 95 % confidence

403 intervals). Figure 3a-2b also indicates that the INP concentrations from the present study agree
 404 well with those reported by Cabrera-Segoviano et al. (2022) for Mexico City and by Chen et al.
 405 (2024) for Beijing (between -19 °C and -22 °C), a polluted megacity such as the MCMA.



406

407

408 Figure 2. INP concentration as a function of temperature for (a) the measurements done
 409 inside performed between the May 16th and to 20th, 2022 period at the northern and southern site
 410 of the Mexico City (MCMA), and (b) literature measurements for the MCMA-MC (2018 and
 411 2019), and Beijing (2017) reported by Cabrera-Segoviano et al. (2022) and Chen et al. (2024)
 412 and Cabrera-Segoviano et al. (2022), respectively. The dark red triangles in (b) panel represent
 413 the INP concentration values reported for 2019 High Pollution Event at South MC (Cabrera-
 414 Segoviano et al., 2022). The error bars represent the carried experimental uncertainty calculated
 415 using the method described in by Mason et al. (2015).3. (a) INP concentrations for the
 416 measurements done on May 20th, 2022 at the northern and southern site, as a function of
 417 temperature; and (b) average INP concentrations for the measurements done at the northern and

418 ~~southern site as a function of temperature. The gray dots, circles, squares, and stars represent~~
419 ~~the INP concentration values reported for Beijing (Chen et al., 2024), 2018 South Mexico City~~
420 ~~(Cabrera Segoviano et al., 2022), 2019 South Mexico City (Cabrera Segoviano et al., 2022),~~
421 ~~2019 High Pollution Event at South Mexico City (Cabrera Segoviano et al., 2022), and 2019~~
422 ~~Southeast Mexico City Metropolitan Area (Rodríguez-Gómez, 2021), respectively. The error~~
423 ~~bars represent the carried experimental uncertainty calculated using the method described by~~
424 ~~Mason et al. (2015).~~

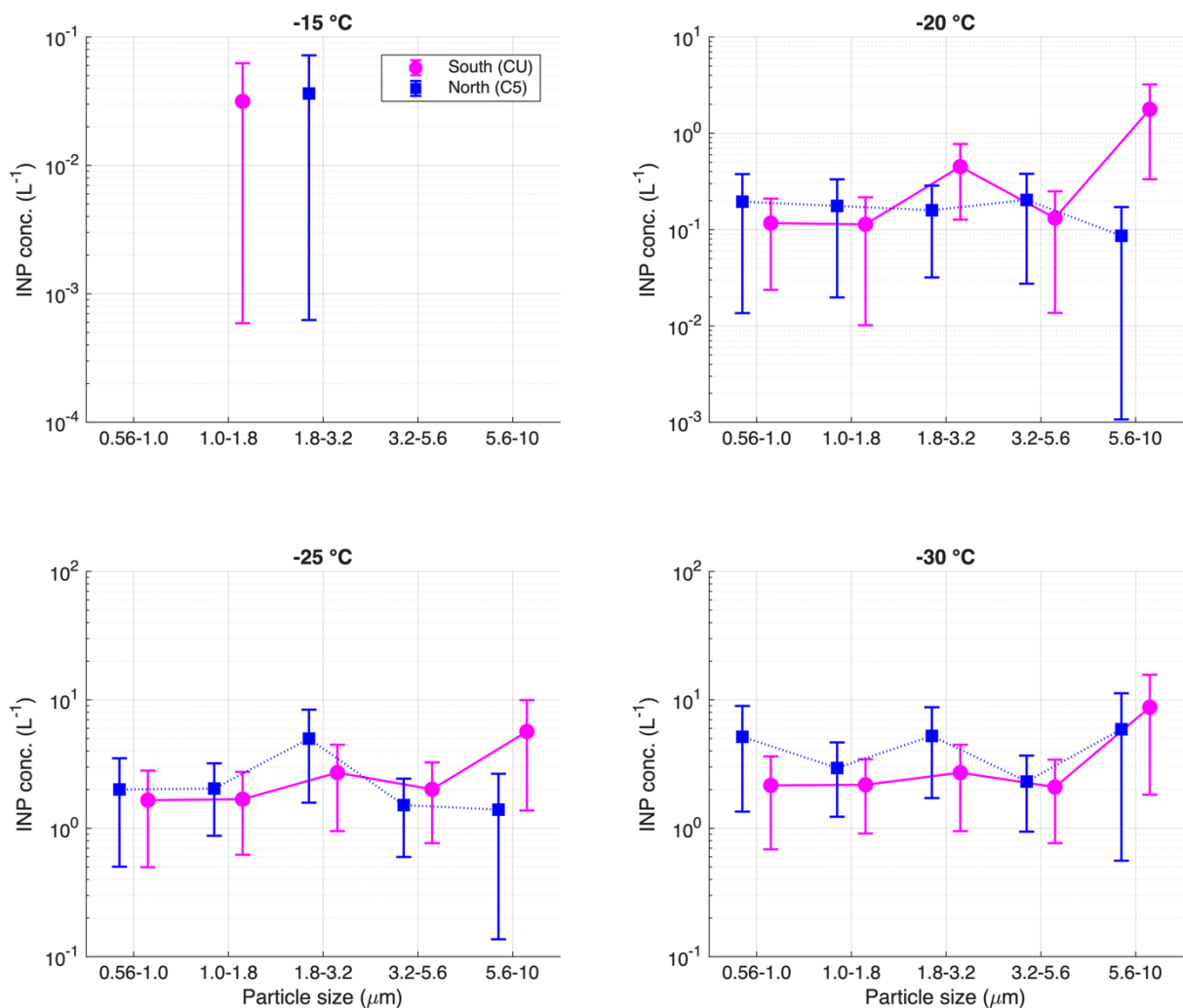
425
426 ~~To better assess the differences in the INP concentration across the two microclimates within~~
427 ~~the MCMA, the average INP concentrations (represented by the average of all samples' total~~
428 ~~INP concentration) for both sites at four different temperatures (15 °C, 20 °C, 25 °C, and 30~~
429 ~~°C) were calculated, as shown in Fig. 3b. INP concentrations at both sampling sites are~~
430 ~~comparable at all temperatures (i.e., 15 °C, 20 °C, 25 °C and 30 °C). Although at 15 °C, a~~
431 ~~clear difference close to one order of magnitude can be observed between both sites (C5 (0.04~~
432 ~~$\pm 0.04 \text{ L}^{-1}$) and CU (0.38 $\pm 0.31 \text{ L}^{-1}$)), the difference is not statistically significant (Agresti and~~
433 ~~Coull, 1998). As shown in Fig. 3b, the INP concentrations measured in the present study agree~~
434 ~~with those reported for southeastern (Rodríguez-Gómez, 2021) and southern sites (Cabrera-~~
435 ~~Segoviano et al., 2022) of the MCMA.~~

436
437 The impact of particle size on the frozen fraction at both sampling sites does not show a clear
438 trend (Fig. S4). Likewise, Fig. 34 shows that the mean INP concentration (which represents the
439 average of all samples for each MOUDI stage) measured on urban particles from the MCMA
440 is not clearly size-dependent. In theory, particle size and INP efficiency are related. This
441 relationship is attributed to surface active sites, as larger particles contain a higher concentration
442 of active sites (Vali, 1996; Hoose and Möhler, 2012; Kanji et al., 2017); however, as urban
443 ambient samples are a complex mixture of particles with different compositions, the
444 relationship between particle size and INP is not straightforward as it requires deeper chemical
445 analysis to understand the heterogeneity in particles chemical composition on each MOUDI stage.

446
447 Even though the particle size did not show a trend, a clear difference is observed at larger
448 particle sizes (i.e., particles between 5.6-10 μm) between the two sampling sites. Showing that
449 the contribution from larger particles to the INP concentrations was found to be greater in the
450 south of the MCMA. Although there is no chemical composition information available for these

451 large particles, we encourage future studies to help understating the importance of PM₁₀
 452 particles.

453 ~~Even though the particle size did not show a trend, a clear difference is observed at larger~~
 454 ~~particle sizes (i.e., particles between 5.6–10 μm) between the two sampling sites. Fig. 2b shows~~
 455 ~~that four of the five samples from stage 2 (i.e., particles between 5.6–10 μm) from the southern~~
 456 ~~site present warmer T₅₀ than the same samples for the northern site. Additionally, the INP~~
 457 ~~average concentrations at -20 °C shows the same behavior as shown in Fig. 4. The contribution~~
 458 ~~from larger particles to the INP concentrations was found to be greater in the south of the~~
 459 ~~MCMA. Although there is no chemical composition information available for these large~~
 460 ~~particles, we encourage future studies to help understating the importance of PM₁₀ particles.~~



461
 462 Figure 34. INP average concentration as a function of particle size at -15 °C, -20 °C, -25 °C,
 463 and -30 °C, for southern (CU, magenta) and northern (C5, blue) MCMA. The error bars
 464 represent the carried experimental uncertainty calculated using the method described by Mason
 465 et al. (2015).

466

467 3.2 Ice nucleation activity vs. criteria pollutants

468 Time series of five criteria pollutant concentrations at both sites are shown in Fig. S2. PM_{2.5}
469 concentration was found to be comparable at both sites, with a slight increase along the last part
470 of the campaign. The maximum difference in PM_{2.5} concentration between both sites was 6.60
471 $\mu\text{g m}^{-3}$. Although high hourly values of PM_{2.5} were measured (in the order of $\sim 60 \mu\text{g m}^{-3}$), they
472 cannot be considered as *high pollution episodes* as was the case described in Cabrera-Segoviano
473 et al. (2022) where PM_{2.5} concentrations above $80 \mu\text{g m}^{-3}$ were measured (Carabali et al., 2021).
474 Similar to previous studies performed within the MCMA, CO, SO₂, and NO_x concentrations
475 were higher at the northern site, with 0.6 ppm, 14 ppm, and 60 ppm maximum difference
476 between the northern and southern sites for CO, SO₂, and NO_x, respectively (Fig. S2). This
477 behavior is related to local emissions, such as gasoline-fueled vehicular emissions and industrial
478 activity (Vega et al., 2004; Castro et al., 2024).

479

480 O₃ concentrations were higher at the southern site (i.e., a 30 ppm maximum difference between
481 both sites). Local emissions from vegetation cover prevalent in southern MCMA, such as
482 volatile organic compounds (VOCs), together with local NO_x emissions and transport can
483 explain the O₃ behavior. It is well known that VOCs may participate in O₃ production by
484 photochemistry and lead to higher concentrations (Pinto et al., 2010; Amador-Muñoz et al.,
485 2016). Therefore, the southern site is likely enriched in biogenic secondary organic aerosols
486 (SOA) compared to the northern site (Aiken et al., 2009; Cooke et al., 2024), with unknown
487 implications in the INP population.

488

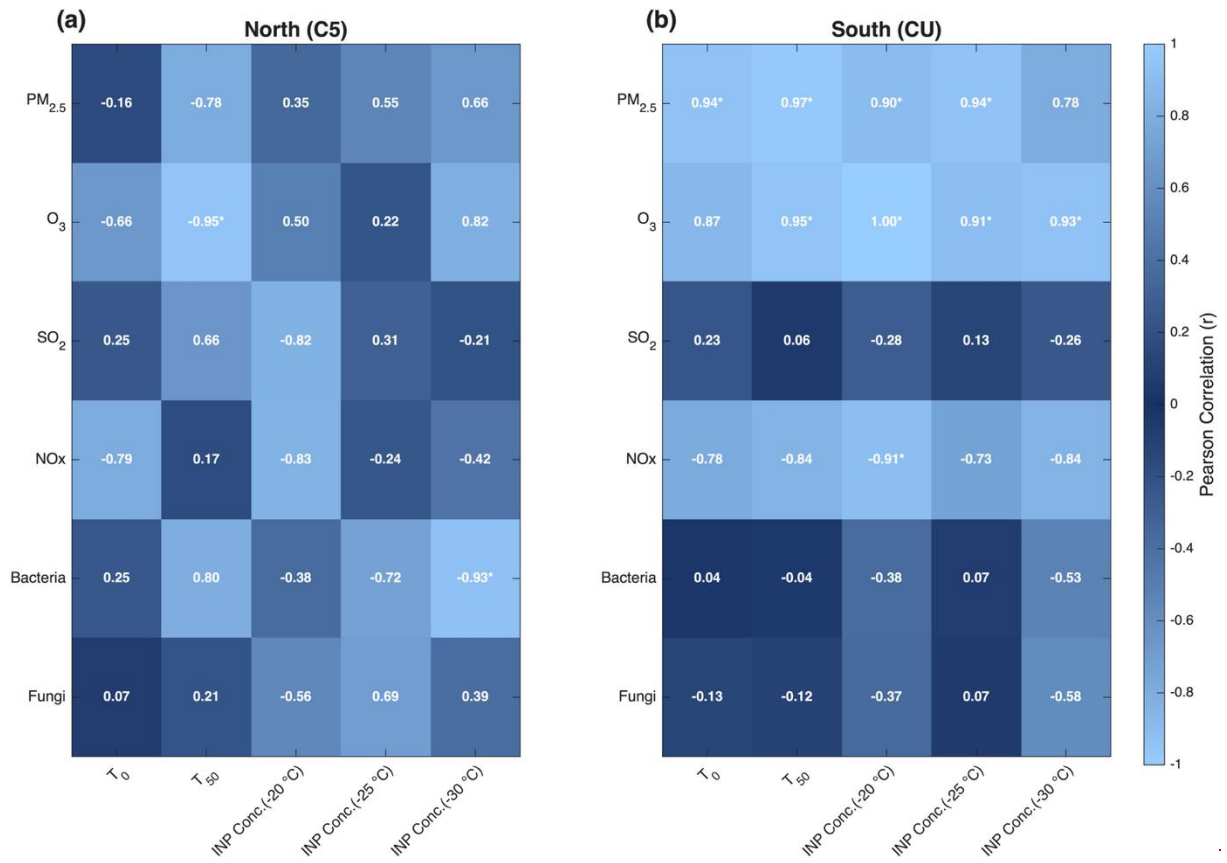
489 The INP concentrations shown in Fig. 23 were comparable at colder temperatures, with a
490 slightly higher concentration at the southern site observed on the last sampling day at warm
491 temperatures. Given that a slight increase in PM_{2.5} concentration was also observed on May
492 20th at the southern site (Fig. S2), there may be a small relationship between INP concentration
493 at warm temperatures and PM_{2.5}. Figure 45 shows the calculated Pearson correlation
494 coefficients between the measured criteria pollutants ~~with T₀, T₅₀~~ and INP concentration at -20
495 °C, -25 °C, and -30 °C for both sampling sites (for particles ranging between 0.56 μm and 3.2
496 μm). Mean criteria pollutant concentrations between 08:00 h and 13:00 h local time were used
497 to match the INP sampling periods. Figure 45 shows high correlations between PM_{2.5}, O₃, and
498 the INP parameters at the southern site, implying that both pollutants can impact the
499 physicochemical properties of the INP population at this site. On the other hand, no significant
500 correlations were found at the northern site. As the INP sizes in both sites are identical, the

501 observed differences are likely linked with differences in the PM_{2.5} composition. As shown in
502 Figs. 56 and S5, the PM_{2.5} elemental and ionic composition in the northern and southern sites
503 have important differences. As the composition is clearly different, the interaction between fine
504 particles, and hence INPs, with O₃ is expected to differ in both sites as well. As the PM_{2.5}
505 sampling time was much larger (24 h) than the 4 h INP sampling, a direct correlation between
506 the elemental and ionic composition with the INP concentrations was not assessed.

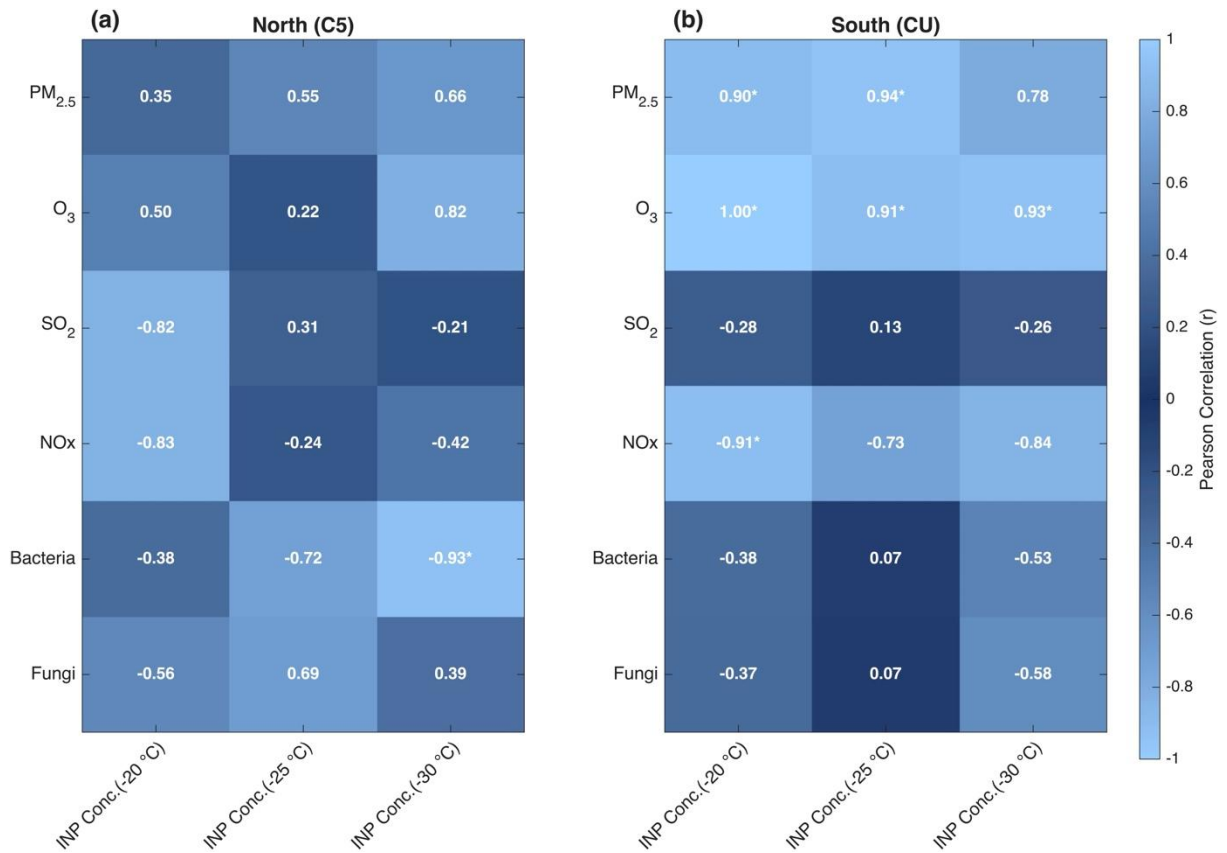
507

508 This suggest that different sources of particles could be present at both MCMA sites, but no
509 correlation was found that anthropogenic pollution could modify INP concentration. The
510 relationship between PM_{2.5} and INP concentrations has been previously evaluated (Chen et al.,
511 2018; Bi et al., 2019; Córdoba et al., 2021; Cabrera-Segoviano et al., 2022), with highly
512 contrasting results, but showing that urban particle concentrations alone do not affect INP
513 concentration.

514



515



516

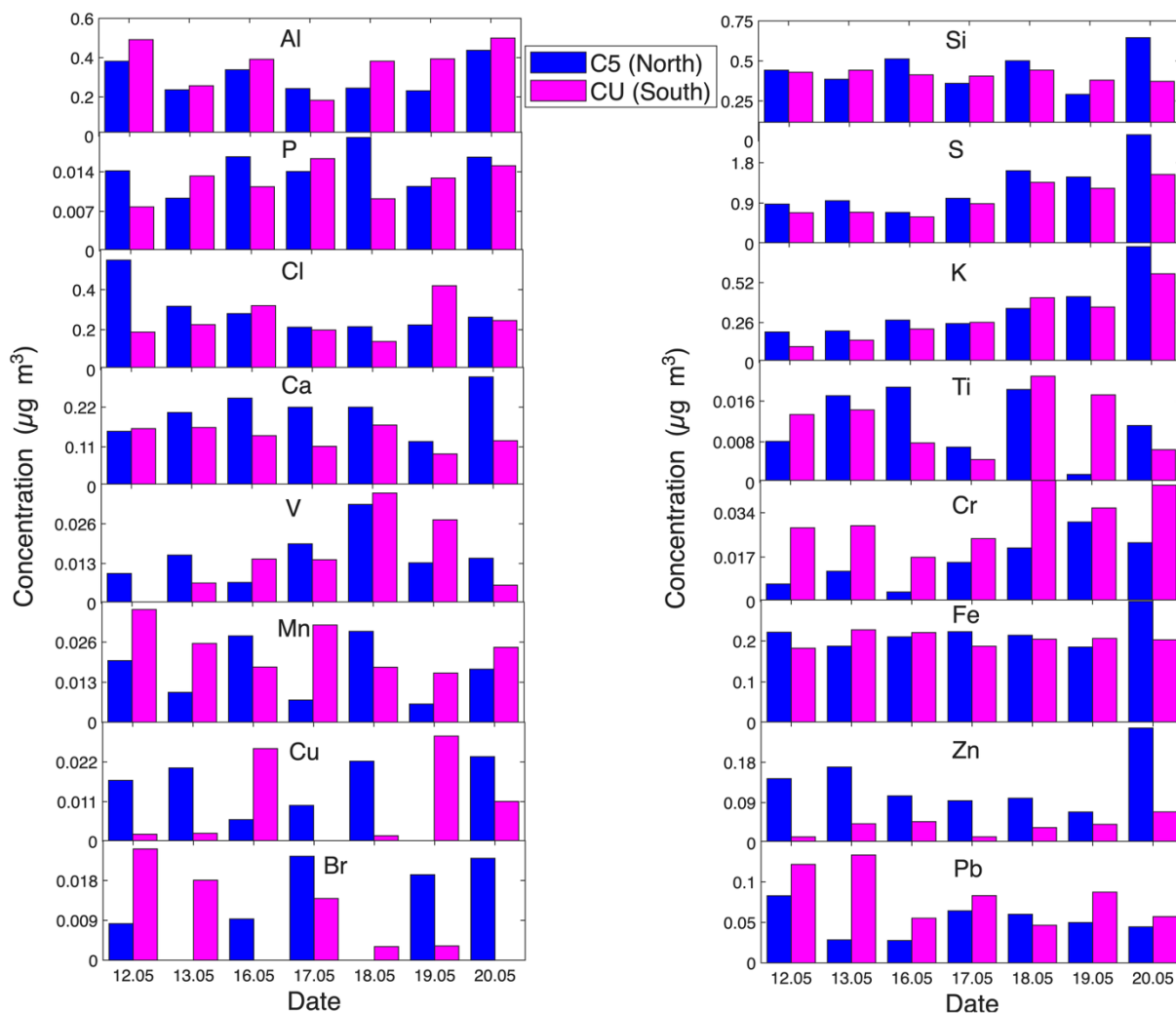
517 Figure 45. Heat map with the Pearson correlation coefficients (r) for the relationships between
 518 the INP parameters (i.e., T_0 , T_{50} , and INP concentrations) at -20 °C, -25 °C and -30 °C) and the

519 ambient criteria pollutants concentrations (i.e., PM_{2.5}, O₃, NO_x, and SO₂) for (a) northern (C5)
520 site and (b) southern (CU) site of the MCMA. Correlation analysis between CO and INP
521 parameters was excluded due to the unavailability of CO data for most INP sampling days~~The~~
522 ~~CO concentration missing data for some INP analysis sampling days explain the absence of~~
523 ~~correlations between INP parameters and CO concentration.~~ The statistically significant
524 coefficients (with 95 % confidence level) are marked with an asterisk.

525

526 The analysis of the elemental composition indicates that the concentration of 12 of the 16
527 analyzed elements (i.e., Si, P, S, Cl, K, Ca, Ti, V, Fe, Cu, Zn, and Br) was higher at the northern
528 site as shown in Fig. 56. The maximum measured concentrations were reported for Al and Si,
529 an indication of the presence of aluminum silicates from resuspended dust, as previously
530 reported (Querol et al., 2019; Córdoba et al., 2021). Pb was present at both sampling sites with
531 a maximum concentration of 0.13 µg m⁻³ and 0.08 µg m⁻³ for CU and C5, respectively. The Pb
532 sources are typically linked with local industrial activities and the usage of low quality fuels
533 (Moreno et al., 2008; Hernández-López et al., 2020). The World Health Organization (WHO)
534 recommends an annual average airborne Pb concentration of 0.5 µg m⁻³ as part of its Global
535 Air Quality Guidelines; therefore, the values reported in this work did not exceed this limit.

536



537

538 Figure 56. Concentration of the different individual elements analyzed by XRF on PM_{2.5} at the
 539 northern (C5, blue) and southern (CU, magenta) sites.

540

541 The maximum S concentration (i.e., 2.42 $\mu\text{g m}^{-3}$) observed in C5 is lower than the values
 542 reported in previous studies (3.24 $\mu\text{g m}^{-3}$, Castro et al., 2024; 3.38 $\mu\text{g m}^{-3}$, IMADA, 1997; 5.10
 543 $\mu\text{g m}^{-3}$, Vega et al., 2004), likely related to differences in the sampling month, but higher than
 544 the highest S concentration reported in CU (i.e., 1.54 $\mu\text{g m}^{-3}$). S and K are markers of high-
 545 pollution events in megacities, typically linked with industrial activity, gasoline combustion,
 546 and BB emissions (Ríos and Raga, 2018; Raga et al., 2021). In this study, a rise in S and K
 547 concentrations during the last sampling day (i.e., May 20th) is clearly observed (Figs. 5 and S5)
 548 and could be attributed to local and regional BB.

549

550 To further explore the chemical composition of urban aerosol particles at both sampling sites,
 551 the ion composition was analyzed. Figure S5 reinforces the significant differences in the urban
 552 particles' chemical composition between the two microclimates. The five analyzed cations

553 (Na⁺, K⁺, Ca²⁺, NH₄⁺, and Mg²⁺) and the three analyzed anions (Cl⁻, NO₃⁻, and SO₄²⁻) showed
554 higher concentrations at the northern site. The relationships among SO₄²⁻, NO₃⁻, and NH₄⁺ at
555 both sampling sites are shown in Tables S3 and S4. The strong observed correlation suggests
556 the presence of (NH₄)₂SO₄ and NH₄NO₃ at both sites, two compounds produced by
557 photochemical reactions driven by gasoline and diesel emissions (Vega et al., 2004; Hernández-
558 López et al., 2020; Castro Romero et al., 2024).

559
560 Figure S6 shows that the HYSPLIT backward trajectories at 250 m AGL at both MCMA sites
561 overlaid on the NASA FIRMS real-time active fire locations for the sampling period (i.e., May
562 12th to May 20th, 2022). Even though not all backward trajectories pass through active fires, the
563 overlap between some back-trajectories and active fires suggests that the local and regional
564 transport of BB particles could contribute to the observed differences in the chemical
565 composition, as shown elsewhere (e.g., Carabali et al., 2021). Additionally, Fig. S6 shows that
566 air-masses in both sampling sites came from very similar directions during the sampling period,
567 so particle transport between two sites cannot be ~~neglected~~despised at all.

568
569 To evaluate potential sources of the measured urban aerosol particles, a cluster analysis was
570 applied using all the chemical species to generate a dendrogram for each sampling site.
571 Hierarchical clustering was conducted using Ward's method, with Pearson correlation
572 coefficients employed as the similarity measure. This technique groups variables by minimizing
573 increases in within-cluster variance, leading to clusters of species with similar temporal
574 patterns. The resulting dendrogram illustrates the level of similarity among variables, where
575 shorter linkage distances represent stronger relationships. Principal cluster components can be
576 linked to a potential source as shown in previous literature analysis of similar samples
577 (Reynoso-Cruces et al., 2023). The dendrogram for the southern site (Fig. S7) presents three
578 groups: the orange cluster with anthropogenic oxidized and non-oxidized species and a
579 contribution of BB regional emissions; the green cluster with geogenic oxidized and non-
580 oxidized species; and the brown cluster with resuspended soil originated from rural areas with
581 geogenic species and some anthropogenic contributions. Likewise, the dendrogram for the
582 northern site (Fig. S8) also shows three groups: the orange cluster, which corresponds to
583 anthropogenic oxidized and non-oxidized species; the blue cluster, containing mostly
584 anthropogenic oxidized species from fossil fuels; and the brown cluster with oxidized and non-
585 oxidized resuspended soils. This cluster analysis highlights the effects of land use and BB on

586 the chemical composition of the urban particles across these two microclimates of the MCMA
587 and denotes sample complexity.

588

589 **3.3 Ice nucleation activity vs. culturable microorganisms**

590 To assess the presence of biological particles at both sampling sites, the concentrations of
591 culturable bacteria and fungi were measured in parallel to the INPs. Significant daily variations

592 in bacteria and fungi concentrations at both sampling sites were observed, as shown in Fig. 67.

593 The measured CFU m⁻³ follow the same pattern at both sites, an inverse pattern with PM_{2.5}

594 concentration. The average concentrations of bacteria and fungi at the northern site were 2774

595 CFU m⁻³ and 433 CFU m⁻³, respectively; at the southern site, the average concentrations of

596 bacteria and fungi were 3882 CFU m⁻³ and 509 CFU m⁻³, respectively. The average bacteria

597 concentrations reported in this study are higher than those reported for Yucatán, México (i.e.,

598 69 CFU m⁻³) (Rodriguez-Gomez et al., 2020), Tijuana, México (i.e., 340 CFU m⁻³) (Hurtado et

599 al., 2014), northwestern Amazon, Colombia (i.e., 228 CFU m⁻³) (Russy-Velandia et al., 2025),

600 and Qingdao, China (i.e., 83 CFU m⁻³) (Li et al., 2011). In contrast, the average fungi

601 concentrations reported in this work are lower than those reported for Yucatán, México (i.e.,

602 1018 CFU m⁻³) (Rodriguez-Gómez et al., 2020), and are consistent with the results reported for

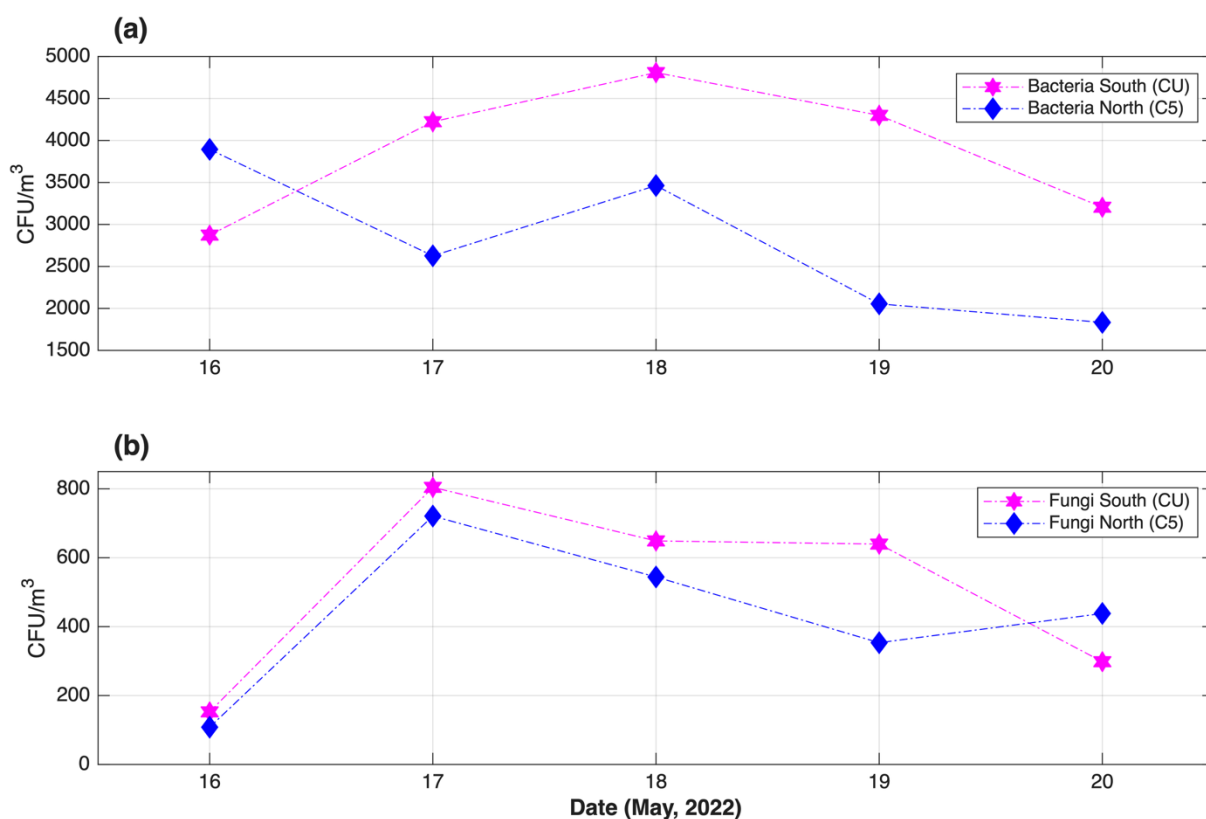
603 northwestern Amazon, Colombia (i.e., 642 CFU m⁻³) (Russy-Velandia et al., 2025) and

604 Qingdao, China (i.e., ~300 CFU m⁻³) (Li et al., 2011). Consistent with the aforementioned

605 studies, the Gram staining analysis indicated that 57 % of the culturable bacteria were Gram-

606 positive

607



608
 609 Figure 67. Time series of the concentration (CFU/m³) of total mesophilic **a)** bacteria and **b)**
 610 fungi measured in the northern (C5, blue) and southern (CU, magenta) sites. ~~As comparison~~
 611 ~~reference, orange markers represent the PM_{2.5} average concentration (μg m⁻³) in both sites.~~

612
 613 A total of 21 bacterial species and eight fungal genera were identified between both sampling
 614 sites (Tables S5 and S6). Although bioparticles were clearly present at both sites, it is doubtful
 615 that they played a key role in the ice nucleating abilities of the collected urban particles. The
 616 FF reported in this work differ significantly with those reported for bioaerosols, typically
 617 showing activation close to -10 °C (Hoose et al., 2010; Knopf et al., 2011; Wex et al., 2015;
 618 Kunert et al., 2019). It is still possible that INP contributed by bioparticles are below the
 619 detection limit of our setup because of sampling methods (i.e., differences in cut-off and total
 620 sampling time). However, an overview of INP concentrations observed in the atmosphere by
 621 Petters and Wright, (2015) indicates that our detection limit of 0.1 L⁻¹ is high enough to enable
 622 the detection of biological particles if they were present. Although the northern site showed
 623 relative higher, but not significant, correlations between microorganisms' concentration and
 624 INP concentrations (Fig. 4), all INP analysis indicate that the identified culturable
 625 microorganisms did not play a primary role in the measured INP concentration of the MCMA
 626 samples. Moreover, the sampling season (dry vegetation season) may be governing the
 627 relationship between biological particles and INP concentration reported here, making it

628 necessary to assess INP concentrations at different times of year (i.e., across meteorological
629 seasons).

630 ~~A total of 21 bacterial species and eight fungal genera were identified between both sampling~~
631 ~~sites (Tables S5 and S6). Although bioparticles were clearly present at both sites, it is doubtful~~
632 ~~that they played a key role in the ice nucleating abilities of the collected urban particles as the~~
633 ~~warmest average T_0 was $(-17.2 \pm 3.8)^\circ\text{C}$. This is very different from the T_0 values reported for~~
634 ~~bioaerosols, typically above -10°C (Hoose et al., 2010; Knopf et al., 2011; Wex et al., 2015;~~
635 ~~Kunert et al., 2019). Although the northern site showed relative higher, but not significant,~~
636 ~~correlations between microorganisms' concentration with INP parameters (Fig. 5), the low T_0~~
637 ~~measured values, compared to other biological INPs, indicate that the identified culturable~~
638 ~~microorganisms did not play a primary role in the measured INP concentration of the MCMA~~
639 ~~samples. Additionally, differences between the biological and INP analysis sampling methods~~
640 ~~(i.e., differences in cut-off and total sampling time) inhibits quantitative correlations.~~

641
642 Although some of the identified bacteria and fungi genera and species have been reported to
643 act as INPs at warm temperatures (Tables S5 and S6), it is completely unknown if the MCMA
644 microorganisms contained the INA protein. Melchum et al. (2023) showed that among the 64
645 analyzed species, the most efficient INP was the *Cupriavidus pauculus* bacteria, with a T_{0an}
646 onset freezing temperature of -11.8°C . Therefore, as demonstrated by Melchum et al. (2023)
647 and previously by Schnell and Vali (1976), tropical biological particles appear to be inefficient
648 INPs. The behavior of bacterial and fungal concentration between the northern and southern
649 sites were evaluated by the Pearson correlation analysis shown in Tables S7 and S8. As
650 expected, mixed values of Pearson coefficients reflect that not all bacteria and fungi found at
651 the southern site (closed to vegetated areas) are present in the northern site.

654 4. Conclusions

655 This work evaluated, for the first time, simultaneous measurements of INP concentration at two
656 sites within one of the largest megacities worldwide. Aerosol particles sampled in the southern
657 and northern parts of the MCMA acted as INPs, via immersion freezing, ~~at average~~
658 ~~temperatures below $(-17.2 \pm 3.8)^\circ\text{C}$ and $(-19.1 \pm 1.5)^\circ\text{C}$, respectively.~~ The average INP
659 concentrations varied between $(0.04 \pm 0.04) \text{ L}^{-1}$ and $(24.9 \pm 18) \text{ L}^{-1}$ at temperatures between -
660 15°C and -30°C . The measured INP concentrations agree with those from previous studies

661 conducted in Mexico City (Mexico) and Beijing (China), showing that INP concentrations are
662 not affected by anthropogenic emissions but are indeed influenced by soil use and other local
663 sources. Although earlier studies have shown that particle size plays a role in the INP
664 concentration of Arctic, urban, marine, biomass burning, and mineral dust particles (e.g., Mason
665 et al., 2016; Córdoba et al, 2020), the present results showed that the INP concentration of
666 complex urban particles from the MCMA are not strongly size-dependent (see Figs. S4 and ~~Fig-~~
667 34).
668

669 The present results clearly demonstrated the existence of microclimates within the MCMA. The
670 INP parameters of the MCMA urban particles correlated with PM_{2.5} and O₃, at the southern
671 site, corroborating that particle mass concentration and ozone concentration are very important
672 for the southern MCMA microclimate. Nevertheless, urban aerosol particles show similar INP
673 concentrations across both sites, suggesting that INP activity does not depend on a specific
674 aerosol type, but rather on the bulk complex mixture of aerosol particles or on the dominance
675 of long-range-transported INPs, with no or only a few additional urban sources. Local
676 emissions and the regional transport of different particles (e.g., BB, biogenic SOA,
677 anthropogenic SOA, mineral dust particles, and bioaerosol), are highlighted as the primary
678 sources of urban aerosol particles along the MCMA. These results are consistent with previous
679 studies in the MCMA that have mostly focused on aerosol chemical composition (Molina et al.,
680 2010; Amador-Muñoz et al., 2011; Ladino et al., 2018).
681

682 Although the distance between both sampling sites is just 16 km, aerosol sources and
683 atmospheric processes linked to particle formation and aerosol aging (e.g., gas-to-particle
684 conversion, organic coatings, and photochemistry) are quite different. This implies key local
685 implications in particle characteristics (i.e., chemical composition, particle morphology, and
686 particle size) that could impact the INP concentration. The present study demonstrates that a
687 larger contribution of unknown large urban aerosol particles (i.e., particles between 5.6-10 μm)
688 could be important for heterogeneous MPC formation at the southern MCMA site, as evidenced
689 by the rise in INP concentration at -20 °C (see Figs. 2 and ~~Fig-~~34). Therefore, if we aim to
690 improve the current understanding of aerosol-cloud interactions within-above this megacity, it
691 is crucial to consider the different microclimates to avoid assuming that aerosol
692 physicochemical and biological characteristics within the megacity are homogeneous. Thus,
693 differences in the local anthropogenic activities, biogenic emissions, population density, and
694 land use are key drivers that must be considered.

695

696 Although the present work shows that air pollutants such as PM_{2.5} and ozone can be linked with
697 the ice nucleating abilities of urban aerosol particles, it is important to understand the role and
698 the origin of the super-micron particles as they are a large contributor to the MCMA INP
699 population.

700

701

702 **Author contributions.** KV, DR, JAC, FC, and LAL performed the field measurements. KV,
703 DR, JAC, FC, SMT, and LAL analyzed the data. GBR and LAL designed the field campaigns
704 and were responsible for funding acquisition. KV, SMT, and EN conducted the INP analysis.
705 OR supported the field campaigns and data acquisition. HA conducted the ionic composition
706 analysis. JM conducted the X-ray fluorescence chemical analysis. JAC, IR, LM, and ES
707 conducted the microorganism's identification analysis. SMT and LAL wrote the paper,
708 addressed the reviews and editing, with contributions from all coauthors.

709

710 **Competing interests.** At least one of authors is part of the Editorial board.

711

712 **Acknowledgments.** The authors thank Alison Ruiz, Maria Isabel Saavedra, Juan Carlos Pineda,
713 and Manuel García for their invaluable help. We thank Miguel Sanchez from the Mexico City
714 Atmospheric Monitoring System for sharing the criteria pollutants data and for his support in
715 using their infrastructure. We also thank the RUOA and PEMBU for sharing their
716 meteorological data. Finally, we thank the NOAA for facilitating the use of the surface maps
717 and HYSPLIT.

718

719 **Financial support.** This research was financially supported by the Consejo Nacional de
720 Humanidades, Ciencia y Tecnología (grant no. 1024827) and the Marcos Moshinsky
721 Foundation. Sebastian Mendoza-Téllez thanks SECIHTI for his PhD fellowship.

722

723 **Data availability.** Data will be made available on request.

724

725 **References**

726 Agresti, A. and Coull, B. A.: Approximate is Better than “Exact” for Interval Estimation of
727 Binomial Proportions, Am. Stat., 52, 119–126,
728 <https://doi.org/10.1080/00031305.1998.10480550>, 1998.

729 [Aiken, A. C., Salcedo, D., Cubison, M. J., Huffman, J. A., DeCarlo, P. F., Ulbrich, I. M.,](#)
730 [Docherty, K. S., Sueper, D., Kimmel, J. R., Worsnop, D. R., Trimborn, A., Northway, M.,](#)
731 [Stone, E. A., Schauer, J. J., Volkamer, R. M., Fortner, E., de Foy, B., Wang, J., Laskin, A.,](#)
732 [Shutthanandan, V., Zheng, J., Zhang, R., Gaffney, J., Marley, N. A., Paredes-Miranda, G.,](#)
733 [Arnott, W. P., Molina, L. T., Sosa, G., and Jimenez, J. L.: Mexico City aerosol analysis during](#)
734 [MILAGRO using high resolution aerosol mass spectrometry at the urban supersite \(T0\) – Part](#)
735 [1: Fine particle composition and organic source apportionment, Atmos Chem Phys,](#)
736 <https://doi.org/10.5194/acp-9-6633-2009>, 2009.

737 [Aldape, F., Flores M., J., Diaz, R. V., Morales, J. R., Cahill, T. A., and Saravia, L.: Seasonal](#)
738 [study of the composition of atmospheric aerosols in Mexico City, Int. J. PIXE, 01, 355–371,](#)
739 <https://doi.org/10.1142/S012908359100024X>, 1991.

740 [Amador-Muñoz, O., Villalobos-Pietrini, R., Miranda, J., and Vera-Avila, L. E.: Organic](#)
741 [compounds of PM_{2.5} in Mexico Valley: Spatial and temporal patterns, behavior and sources,](#)
742 [Sci. Total Environ., 409, 1453–1465, https://doi.org/10.1016/j.scitotenv.2010.11.026](#), 2011.

743 [Amador-Muñoz, O., Bazán-Torija, S., Villa-Ferreira, S. A., Villalobos-Pietrini, R., Bravo-](#)
744 [Cabrera, J. L., Munive-Colín, Z., Hernández-Mena, L., Saldarriaga-Noreña, H., and Murillo-](#)
745 [Tovar, M. A.: Opposing seasonal trends for polycyclic aromatic hydrocarbons and PM₁₀:](#)
746 [Health risk and sources in southwest Mexico City, Atmospheric Res., 122, 199–212,](#)
747 <https://doi.org/10.1016/j.atmosres.2012.10.003>, 2013.

748 [Amador-Muñoz, O., Misztal, P. K., Weber, R., Worton, D. R., Zhang, H., Drozd, G., and](#)
749 [Goldstein, A. H.: Sensitive detection of *n*-alkanes using a mixed ionization mode proton-](#)
750 [transfer-reaction mass spectrometer, Atmospheric Meas. Tech., 9, 5315–5329,](#)
751 <https://doi.org/10.5194/amt-9-5315-2016>, 2016.

752 [Behzadi, F., Wasti, A., Haque Rahat, S., Tracy, J. N., and Ray, P. A.: Analysis of the climate](#)
753 [change signal in Mexico City given disagreeing data sources and scattered projections, J.](#)
754 [Hydrol. Reg. Stud., 27, 100662, https://doi.org/10.1016/j.ejrh.2019.100662](#), 2020.

755 [Bi, K., McMeeking, G. R., Ding, D. P., Levin, E. J. T., DeMott, P. J., Zhao, D. L., Wang, F.,](#)
756 [Liu, Q., Tian, P., Ma, X. C., Chen, Y. B., Huang, M. Y., Zhang, H. L., Gordon, T. D., and Chen,](#)
757 [P.: Measurements of Ice Nucleating Particles in Beijing, China, J. Geophys. Res. Atmospheres,](#)
758 [124, 8065–8075, https://doi.org/10.1029/2019JD030609](#), 2019.

759 [Burrows, S. M., McCluskey, C. S., Cornwell, G., Steinke, I., Zhang, K., Zhao, B., Zawadowicz,](#)
760 [M., Raman, A., Kulkarni, G., China, S., Zelenyuk, A., and DeMott, P. J.: Ice-Nucleating](#)
761 [Particles That Impact Clouds and Climate: Observational and Modeling Research Needs, Rev.](#)
762 [Geophys., 60, e2021RG000745, https://doi.org/10.1029/2021RG000745](#), 2022.

763 [Cabrera-Segoviano, D., Pereira, D. L., Rodriguez, C., Raga, G. B., Miranda, J., Alvarez-Ospina,](#)
764 [H., and Ladino, L. A.: Inter-annual variability of ice nucleating particles in Mexico City, Atmos.](#)
765 [Environ., 273, 118964, https://doi.org/10.1016/j.atmosenv.2022.118964](#), 2022.

766 [Carabali, G., Villanueva-Macias, J., Ladino, L. A., Álvarez-Ospina, H., Raga, G. B., Andraca-](#)
767 [Ayala, G., Miranda, J., Grutter, M., Silva, Ma. M., and Riveros-Rosas, D.: Characterization of](#)
768 [aerosol particles during a high pollution episode over Mexico City, Sci. Rep., 11, 22533,](#)
769 <https://doi.org/10.1038/s41598-021-01873-4>, 2021.

770 [Castro Romero, T., Peralta, O., Prieto, C., Santiago, N., Alvarez-Ospina, H., García Martínez,](#)
771 [R., Saavedra Rosado, I., Espinosa Fuentes, M. D. L. L., Hernández, E., Miranda, J., Gómez, V.,](#)
772 [Solís, C., Salcedo, D., Torres-Jardón, R., Martínez-Arroyo, A., Ortíz Álvarez, A., Ruíz-](#)
773 [Suárez, G., and Ortiz, E.: Characterization of PM_{2.5} during ACU15 campaign in Mexico City,](#)
774 [Geofísica Int., 63, 1225–1238, <https://doi.org/10.22201/igeof.2954436xe.2024.63.4.1745>,](#)
775 [2024.](#)

776 [Celada-Murillo, A.-T., Carreón-Sierra, S., Salcido, A., Castro, T., Peralta, O., and Georgiadis,](#)
777 [T.: Main Characteristics of Mexico City Local Wind Events during the MILAGRO 2006](#)
778 [Campaign within a Meso- \$\beta\$ Scale Lattice Wind Modeling Approach, ISRN Meteorol., 2013,](#)
779 [1–14, <https://doi.org/10.1155/2013/605210>, 2013.](#)

780 [Chen, J., Wu, Z., Augustin-Bauditz, S., Grawe, S., Hartmann, M., Pei, X., Liu, Z., Ji, D., and](#)
781 [Wex, H.: Ice-nucleating particle concentrations unaffected by urban air pollution in Beijing,](#)
782 [China, Atmospheric Chem. Phys., 18, 3523–3539, <https://doi.org/10.5194/acp-18-3523-2018>,](#)
783 [2018.](#)

784 [Chen, J., Wu, Z., Gong, X., Qiu, Y., Chen, S., Zeng, L., and Hu, M.: Anthropogenic Dust as a](#)
785 [Significant Source of Ice-Nucleating Particles in the Urban Environment, Earths Future, 12,](#)
786 [e2023EF003738, <https://doi.org/10.1029/2023EF003738>, 2024.](#)

787 [Cooke, M. E., Waters, C. M., Asare, J. Y., Mirrielees, J. A., Holen, A. L., Frauenheim, M. P.,](#)
788 [Zhang, Z., Gold, A., Pratt, K. A., Surratt, J. D., Ladino, L. A., and Ault, A. P.: Atmospheric](#)
789 [Aerosol Sulfur Distribution and Speciation in Mexico City: Sulfate, Organosulfates, and](#)
790 [Isoprene-Derived Secondary Organic Aerosol from Low NO Pathways, ACS EST Air, 1, 1037–](#)
791 [1052, <https://doi.org/10.1021/acsestair.4c00048>, 2024.](#)

792 [Córdoba, F., Ramírez-Romero, C., Cabrera, D., Raga, G. B., Miranda, J., Alvarez-Ospina, H.,](#)
793 [Rosas, D., Figueroa, B., Kim, J. S., Yakobi-Hancock, J., Amador, T., Gutierrez, W., García,](#)
794 [M., Bertram, A. K., Baumgardner, D., and Ladino, L. A.: Measurement report: Ice nucleating](#)
795 [abilities of biomass burning, African dust, and sea spray aerosol particles over the Yucatán](#)
796 [Peninsula, Atmospheric Chem. Phys., 21, 4453–4470, \[https://doi.org/10.5194/acp-21-4453-\]\(https://doi.org/10.5194/acp-21-4453-2021\)](#)
797 [2021, 2021.](#)

798 [Doran, J. C., Arnott, W. P., Barnard, J. C., Cary, R., Coulter, R., Fast, J. D., Kassianov, E. I.,](#)
799 [Kleinman, L., Laulainen, N. S., Martin, T., Paredes-Miranda, G., Pekour, M. S., Shaw, W. J.,](#)
800 [Smith, D. F., and Springston, S. R.: The T1-T2 study: evolution of aerosol properties downwind](#)
801 [of Mexico City, Atmospheric Chem. Phys. Discuss., 6 \(6\), 12967-12999.,](#)
802 [https://doi.org/10.5194/acp-7-1585-2007, 2007.](#)

803 [Draxler, R.R., R., G. D.: HYSPLIT \(HYbrid Single-Particle Lagrangian Integrated Trajectory\)](#)
804 [Model, 2010.](#)

805 [Edgerton, S. A., Bian, X., Doran, J. C., Fast, J. D., Hubbe, J. M., Malone, E. L., Shaw, W. J.,](#)
806 [Whiteman, C. D., Zhong, S., Arriaga, J. L., Ortiz, E., Ruiz, M., Sosa, G., Vega, E., Limon, T.,](#)
807 [Guzman, F., Archuleta, J., Bossert, J. E., Elliot, S. M., Lee, J. T., McNair, L. A., Chow, J. C.,](#)
808 [Watson, J. G., Coulter, R. L., Doskey, P. V., Gaffney, J. S., Marley, N. A., Neff, W., and Petty,](#)
809 [R.: Particulate Air Pollution in Mexico City: A Collaborative Research Project, J. Air Waste](#)
810 [Manag. Assoc., 49, 1221–1229, <https://doi.org/10.1080/10473289.1999.10463915>, 1999.](#)

811 [Espinosa, A., Miranda, J., and Pineda, J.C: Uncertainty evaluation in correlated quantities:](#)
812 [application to elemental analysis of atmospheric aerosols, Rev. Mex. Física, 56 \(1\), 134–140,](#)
813 [2010.](#)

814 [Espinosa, A. A., Reyes-Herrera, J., Miranda, J., Mercado, F., Veytia, M. A., Cuautle, M., and](#)
815 [Cruz, J. I.: Development of an X-ray fluorescence spectrometer for environmental science](#)
816 [applications, Instrum. Sci. Technol., 40, 603–617,](#)
817 <https://doi.org/10.1080/10739149.2012.693560>, 2012.

818 [Gimeno, L., Sorí, R., Vázquez, M., Stojanovic, M., Algarra, I., Eiras-Barca, J., Gimeno-Sotelo,](#)
819 [L., and Nieto, R.: Extreme precipitation events, WIREs Water, 9, e1611,](#)
820 <https://doi.org/10.1002/wat2.1611>, 2022.

821 [Hasenkopf, C. A., Veghte, D. P., Schill, G. P., Lodoysamba, S., Freedman, M. A., and Tolbert,](#)
822 [M. A.: Ice nucleation, shape, and composition of aerosol particles in one of the most polluted](#)
823 [cities in the world: Ulaanbaatar, Mongolia, Atmos. Environ., 139, 222–229,](#)
824 <https://doi.org/10.1016/j.atmosenv.2016.05.037>, 2016.

825 [Hernández-López, A. E., Miranda Martín Del Campo, J., Mugica-Álvarez, V., Hernández-](#)
826 [Valle, B. L., Mejía-Ponce, L. V., Pineda-Santamaría, J. C., Reynoso-Cruces, S., Mendoza-](#)
827 [Flores, J. A., and Rozanes-Valenzuela, D.: A study of PM_{2.5} elemental composition in](#)
828 [southwest Mexico City and development of receptor models with positive matrix factorization,](#)
829 [Rev. Int. Contam. Ambient., https://doi.org/10.20937/RICA.54066](#), 2020.

830 [Hernández-López, A. E., Santos-Medina, G. L., Morton-Bermea, O., Hernández-Álvarez, E.,](#)
831 [Villalobos-Pietrini, R., and Amador-Muñoz, O.: Chemical speciation of organic compounds](#)
832 [and elemental compositions of PM_{2.5} in Mexico City: Spatial-seasonal distribution, emission](#)
833 [sources, and formation processes, Atmospheric Res., 292, 106868,](#)
834 <https://doi.org/10.1016/j.atmosres.2023.106868>, 2023.

835 [Heymsfield, A. J., Schmitt, C., Chen, C.-C.-J., Bansemer, A., Gettelman, A., Field, P. R., and](#)
836 [Liu, C.: Contributions of the Liquid and Ice Phases to Global Surface Precipitation:](#)
837 [Observations and Global Climate Modeling, J. Atmospheric Sci., 77, 2629–2648,](#)
838 <https://doi.org/10.1175/JAS-D-19-0352.1>, 2020.

839 [Hoose, C. and Möhler, O.: Heterogeneous ice nucleation on atmospheric aerosols: a review of](#)
840 [results from laboratory experiments, Atmospheric Chem. Phys., 12, 9817–9854,](#)
841 <https://doi.org/10.5194/acp-12-9817-2012>, 2012.

842 [Hoose, C., Kristjánsson, J. E., and Burrows, S. M.: How important is biological ice nucleation](#)
843 [in clouds on a global scale?, Environ. Res. Lett., 5, 024009, https://doi.org/10.1088/1748-](#)
844 [9326/5/2/024009](#), 2010.

845 [Houze, R. A.: Cloud dynamics, Second edition., Academic Press, Oxford, England, 2014.](#)

846 [Hurtado, L., Rodríguez, G., López, J., Castillo, J. E., Molina, L., Zavala, M., and Quintana, P.](#)
847 [J. E.: Characterization of atmospheric bioaerosols at 9 sites in Tijuana, Mexico, Atmos.](#)
848 [Environ., 96, 430–436, https://doi.org/10.1016/j.atmosenv.2014.07.018](#), 2014.

849 [Población: https://www.inegi.org.mx/temas/estructura/, last access: 10 October 2025.](#)

850 Jahl, L. G., Brubaker, T. A., Polen, M. J., Jahn, L. G., Cain, K. P., Bowers, B. B., Fahy, W. D.,
851 Graves, S., and Sullivan, R. C.: Atmospheric aging enhances the ice nucleation ability of
852 biomass-burning aerosol, *Sci. Adv.*, 7, <https://doi.org/10.1126/sciadv.abd3440>, 2021.

853 Jahn, L. G., Polen, M. J., Jahl, L. G., Brubaker, T. A., Somers, J., and Sullivan, R. C.: Biomass
854 combustion produces ice-active minerals in biomass-burning aerosol and bottom ash, *Proc.*
855 *Natl. Acad. Sci.*, 117, 21928–21937, <https://doi.org/10.1073/pnas.1922128117>, 2020.

856 Jáuregui, E.: El clima de la Ciudad de México, 1. ed., Instituto de Geografía, UNAM: Plaza y
857 Valdés Editores, México, D.F, 131 pp., 2000.

858 Kanji, Z. A., Ladino, L. A., Wex, H., Boose, Y., Burkert-Kohn, M., Cziczo, D. J., and Krämer,
859 M.: Overview of Ice Nucleating Particles, *Meteorol. Monogr.*, 58, 1.1-1.33,
860 <https://doi.org/10.1175/AMSMONOGRAPHS-D-16-0006.1>, 2017.

861 Knopf, D. A., Wang, B., Laskin, A., Moffet, R. C., and Gilles, M. K.: Heterogeneous nucleation
862 of ice on anthropogenic organic particles collected in Mexico City, *Geophys. Res. Lett.*, 37,
863 2010GL043362, <https://doi.org/10.1029/2010GL043362>, 2010.

864 Knopf, D. A., Alpert, P. A., Wang, B., and Aller, J. Y.: Stimulation of ice nucleation by marine
865 diatoms, *Nat. Geosci.*, 4, 88–90, <https://doi.org/10.1038/ngeo1037>, 2011.

866 Kunert, A. T., Pöhlker, M. L., Tang, K., Krevert, C. S., Wieder, C., Speth, K. R., Hanson, L.
867 E., Morris, C. E., Schmale Iii, D. G., Pöschl, U., and Fröhlich-Nowoisky, J.: Macromolecular
868 fungal ice nuclei in *Fusarium*: effects of physical and chemical processing, *Biogeosciences*,
869 16, 4647–4659, <https://doi.org/10.5194/bg-16-4647-2019>, 2019.

870 Ladino, L. A., Raga, G. B., and Baumgardner, D.: On particle-bound polycyclic aromatic
871 hydrocarbons (PPAH) and links to gaseous emissions in Mexico City, *Atmos. Environ.*, 194,
872 31–40, <https://doi.org/10.1016/j.atmosenv.2018.09.022>, 2018.

873 Lezama, J. L. and Vargas, V. I.: Las fuerzas rectoras de la contaminación del aire en la Ciudad
874 de México, MIT Integr. Program Urban Reg. Glob. Air Pollut. Rep. NO8 Camb. MA, 2000.

875 Li, C., Zwiers, F., Zhang, X., Chen, G., Lu, J., Li, G., Norris, J., Tan, Y., Sun, Y., and Liu,
876 M.: Larger Increases in More Extreme Local Precipitation Events as Climate Warms,
877 *Geophys. Res. Lett.*, 46, 6885–6891, <https://doi.org/10.1029/2019GL082908>, 2019.

878 Li, M., Qi, J., Zhang, H., Huang, S., Li, L., and Gao, D.: Concentration and size distribution of
879 bioaerosols in an outdoor environment in the Qingdao coastal region, *Sci. Total Environ.*, 409,
880 3812–3819, <https://doi.org/10.1016/j.scitotenv.2011.06.001>, 2011.

881 Mason, R. H., Chou, C., McCluskey, C. S., Levin, E. J. T., Schiller, C. L., Hill, T. C. J.,
882 Huffman, J. A., DeMott, P. J., and Bertram, A. K.: The micro-orifice uniform deposit impactor–
883 droplet freezing technique (MOUDI-DFT) for measuring concentrations of ice nucleating
884 particles as a function of size: improvements and initial validation, *Atmospheric Meas. Tech.*,
885 8, 2449–2462, <https://doi.org/10.5194/amt-8-2449-2015>, 2015.

886 Mason, R. H., Si, M., Chou, C., Irish, V. E., Dickie, R., Elizondo, P., Wong, R., Brintnell, M.,
887 Elsasser, M., Lassar, W. M., Pierce, K. M., Leaitch, W. R., MacDonald, A. M., Platt, A., Toom-
888 Sauntry, D., Sarda-Estève, R., Schiller, C. L., Suski, K. J., Hill, T. C. J., Abbatt, J. P. D.,
889 Huffman, J. A., DeMott, P. J., and Bertram, A. K.: Size-resolved measurements of ice-

890 [nucleating particles at six locations in North America and one in Europe, Atmospheric Chem.](#)
891 [Phys., 16, 1637–1651, https://doi.org/10.5194/acp-16-1637-2016, 2016.](#)

892 [Melchum, A., Córdoba, F., Salinas, E., Martínez, L., Campos, G., Rosas, I., Garcia-Mendoza,](#)
893 [E., Olivos-Ortiz, A., Raga, G. B., Pizano, B., Silva, Ma. M., and Ladino, L. A.: Maritime and](#)
894 [continental microorganisms collected in Mexico: An investigation of their ice-nucleating](#)
895 [abilities, Atmospheric Res., 293, 106893, https://doi.org/10.1016/j.atmosres.2023.106893,](#)
896 [2023.](#)

897 [Met Office, 2023, "Microclimates," National Meteorological Library and Archive Factsheet 14,](#)
898 [https://www.metoffice.gov.uk/binaries/content/assets/metofficegovuk/pdf/research/library-](#)
899 [and-archive/library/publications/factsheets/factsheet_14-microclimates_2023.pdf, last access:](#)
900 [17 February 2026.](#)

901 [Molina, H., Yang, Y., Ruch, T., Kim, J.-W., Mortensen, P., Otto, T., Nalli, A., Tang, Q.-Q.,](#)
902 [Lane, M. D., Chaerkady, R., and Pandey, A.: Temporal Profiling of the Adipocyte Proteome](#)
903 [during Differentiation Using a Five-Plex SILAC Based Strategy, J. Proteome Res., 8, 48–58,](#)
904 [https://doi.org/10.1021/pr800650r, 2009.](#)

905 [Molina, L. T., Madronich, S., Gaffney, J. S., Apel, E., De Foy, B., Fast, J., Ferrare, R., Herndon,](#)
906 [S., Jimenez, J. L., Lamb, B., Osornio-Vargas, A. R., Russell, P., Schauer, J. J., Stevens, P. S.,](#)
907 [Volkamer, R., and Zavala, M.: An overview of the MILAGRO 2006 Campaign: Mexico City](#)
908 [emissions and their transport and transformation, Atmospheric Chem. Phys., 10, 8697–8760,](#)
909 [https://doi.org/10.5194/acp-10-8697-2010, 2010.](#)

910 [Molina, M. J. and Molina, L. T.: Megacities and Atmospheric Pollution, J. Air Waste Manag.](#)
911 [Assoc., 54, 644–680, https://doi.org/10.1080/10473289.2004.10470936, 2004.](#)

912 [Moreno, T., Querol, X., Pey, J., Minguillón, M. C., Pérez, N., Alastuey, A., Bernabé, R. M.,](#)
913 [Blanco, S., Cárdenas, B., Eichinger, W., Salcido, A., and Gibbons, W.: Spatial and temporal](#)
914 [variations in inhalable CuZnPb aerosols within the Mexico City pollution plume, J. Environ.](#)
915 [Monit., 10, 370, https://doi.org/10.1039/b716507b, 2008.](#)

916 [Mülmenstädt, J., Sourdeval, O., Delanoë, J., and Quaas, J.: Frequency of occurrence of rain](#)
917 [from liquid-, mixed-, and ice-phase clouds derived from A-Train satellite retrievals, Geophys.](#)
918 [Res. Lett., 42, 6502–6509, https://doi.org/10.1002/2015GL064604, 2015.](#)

919 [Ohneiser, K., Seifert, P., Schimmel, W., Senf, F., Gaudek, T., Radenz, M., Teisseire, A.,](#)
920 [Ettrichrätz, V., Vogl, T., Maherndl, N., Pfeifer, N., Henneberger, J., Miller, A. J., Omanovic,](#)
921 [N., Fuchs, C., Zhang, H., Ramelli, F., Spirig, R., Kötsche, A., Kalesse-Los, H., Maahn, M.,](#)
922 [Corden, H., Berne, A., Hajipour, M., Griesche, H., Hofer, J., Engelmann, R., Skupin, A.,](#)
923 [Ansmann, A., and Baars, H.: Impact of seeder-feeder cloud interaction on precipitation](#)
924 [formation: a case study based on extensive remote-sensing, in situ and model data, Atmospheric](#)
925 [Chem. Phys., 25, 17363–17386, https://doi.org/10.5194/acp-25-17363-2025, 2025.](#)

926 [Pereira, D. L., Silva, Ma. M., García, R., Raga, G. B., Alvarez-Ospina, H., Carabali, G., Rosas,](#)
927 [I., Martinez, L., Salinas, E., Hidalgo-Bonilla, S., and Ladino, L. A.: Characterization of ice](#)
928 [nucleating particles in rainwater, cloud water, and aerosol samples at two different tropical](#)
929 [latitudes, Atmospheric Res., 250, 105356, https://doi.org/10.1016/j.atmosres.2020.105356,](#)
930 [2021.](#)

931 [Petters, M. D. and Wright, T. P.: Revisiting ice nucleation from precipitation samples: ICE](#)
932 [NUCLEATION FROM PRECIPITATION, Geophys. Res. Lett., 42, 8758–8766,](#)
933 <https://doi.org/10.1002/2015GL065733>, 2015.

934 [Pinto, D. M., Blande, J. D., Souza, S. R., Nerg, A.-M., and Holopainen, J. K.: Plant Volatile](#)
935 [Organic Compounds \(VOCs\) in Ozone \(O₃\) Polluted Atmospheres: The Ecological Effects, J.](#)
936 [Chem. Ecol., 36, 22–34, https://doi.org/10.1007/s10886-009-9732-3](#), 2010.

937 [Prenni, A. J., DeMott, P. J., Sullivan, A. P., Sullivan, R. C., Kreidenweis, S. M., and Rogers,](#)
938 [D. C.: Biomass burning as a potential source for atmospheric ice nuclei: Western wildfires and](#)
939 [prescribed burns, Geophys. Res. Lett., 39, https://doi.org/10.1029/2012gl051915](#), 2012.

940 [Purdy, J. C., Austin, G. L., Seed, A. W., and Cluckie, I. D.: Radar evidence of orographic](#)
941 [enhancement due to the seeder feeder mechanism, Meteorol. Appl., 12, 199–206,](#)
942 <https://doi.org/10.1017/S1350482705001672>, 2005.

943 [Querol, X., Pey, J., Minguillón, M. C., Pérez, N., Alastuey, A., Viana, M., Moreno, T., Bernabé,](#)
944 [R. M., Blanco, S., Cárdenas, B., Vega, E., Sosa, G., Escalona, S., Ruiz, H., and Artíñano, B.:](#)
945 [PM speciation and sources in Mexico during the MILAGRO-2006 Campaign, Atmospheric](#)
946 [Chem. Phys., 8, 111–128, https://doi.org/10.5194/acp-8-111-2008](#), 2008.

947 [Querol, X., Tobías, A., Pérez, N., Karanasiou, A., Amato, F., Stafoggia, M., Pérez García-](#)
948 [Pando, C., Ginoux, P., Forastiere, F., Gumy, S., Mudu, P., and Alastuey, A.: Monitoring the](#)
949 [impact of desert dust outbreaks for air quality for health studies, Environ. Int., 130, 104867,](#)
950 <https://doi.org/10.1016/j.envint.2019.05.061>, 2019.

951 [Raga, G. B., Ladino, L. A., Baumgardner, D., Ramirez-Romero, C., Córdoba, F., Alvarez-](#)
952 [Ospina, H., Rosas, D., Amador, T., Miranda, J., Rosas, I., Jaramillo, A., Yakobi-Hancock, J.,](#)
953 [Kim, J. S., Martínez, L., Salinas, E., and Figueroa, B.: ADABBOY: African Dust And Biomass](#)
954 [Burning Over Yucatan, Bull. Am. Meteorol. Soc., 102, E1543–E1556,](#)
955 <https://doi.org/10.1175/BAMS-D-20-0172.1>, 2021.

956 [Reynoso-Cruces, S., Miranda-Martín-Del-Campo, J., and Pineda-Santamaría, J. C.: Elemental](#)
957 [composition of PM₁₀ in indoor environments of a scientific research institution and risk](#)
958 [assessment, Environ. Pollut. Bioavail., 35, 2232108,](#)
959 <https://doi.org/10.1080/26395940.2023.2232108>, 2023.

960 [Riojas-Rodríguez, H., Álamo-Hernández, U., Texcalac-Sangrador, J. L., and Romieu, I.: Health](#)
961 [impact assessment of decreases in PM₁₀ and ozone concentrations in the Mexico City](#)
962 [Metropolitan Area. A basis for a new air quality management program, Salud Pública México,](#)
963 [56, 579, https://doi.org/10.21149/spm.v56i6.7384](#), 2014.

964 [Ríos, B. and Raga, G. B.: Spatio-temporal distribution of burned areas by ecoregions in Mexico](#)
965 [and Central America, Int. J. Remote Sens., 39, 949–970,](#)
966 <https://doi.org/10.1080/01431161.2017.1392641>, 2018.

967 [Rodríguez-Gómez, C.: Variabilidad de los núcleos de glaciación en la capa límite y la tropósfera](#)
968 [libre en Alzomoni, y su influencia en la formación de nubes mixtas, Universidad Nacional](#)
969 [Autónoma de México, México, CDMX, 128 pp., 2021.](#)

970 [Rodriguez-Gomez, C., Ramirez-Romero, C., Cordoba, F., Raga, G. B., Salinas, E., Martinez,](#)
971 [L., Rosas, I., Quintana, E. T., Maldonado, L. A., Rosas, D., Amador, T., Alvarez, H., and](#)

972 Ladino, L. A.: Characterization of culturable airborne microorganisms in the Yucatan
973 Peninsula, Atmos. Environ., 223, 117183, <https://doi.org/10.1016/j.atmosenv.2019.117183>,
974 2020.

975 Rogers, R. R. and Yau, M. K.: A short course in cloud physics, Third edition., Butterworth-
976 Heinemann, Burlington, Massachusetts, 1 pp., 1996.

977 Rosas, D., Silva, M. M., Figueroa, B., Morton-Bermea, O., Miranda, J., Alvarez, H., Puig, T.
978 P., Morales, J., Uuh, J., Hernández-Alvarez, E., Novelo, S., Olivares, J., Salcedo, D., Rosas, I.,
979 Ponce, C., Raga, G. B., and Ladino, L. A.: African dust particles over the western Caribbean:
980 Chemical characterization, Atmos. Environ., 347, 121095,
981 <https://doi.org/10.1016/j.atmosenv.2025.121095>, 2025.

982 Russy-Velandia, L., Ramírez, O., Barrera, J., Mendoza-Téllez, S., Álvarez, H., Patiño, M. C.,
983 and Ladino, L. A.: Approach to culturable bioaerosols and their environmental drivers at a
984 border site in the northwestern Amazon, Atmospheric Environ. X, 27, 100362,
985 <https://doi.org/10.1016/j.aeaoa.2025.100362>, 2025.

986 Salcido, A., Carreón-Sierra, S., Georgiadis, T., Celada-Murillo, A.-T., and Castro, T.: Lattice
987 Wind Description and Characterization of Mexico City Local Wind Events in the 2001–2006
988 Period, Climate, 3, 542–562, <https://doi.org/10.3390/cli3030542>, 2015.

989 Schnell, R. C. and Vali, G.: Biogenic Ice Nuclei: Part I. Terrestrial and Marine Sources, J.
990 Atmospheric Sci., 33, 1554–1564, [https://doi.org/10.1175/1520-](https://doi.org/10.1175/1520-0469(1976)033%253C1554:BINPIT%253E2.0.CO;2)
991 0469(1976)033%253C1554:BINPIT%253E2.0.CO;2, 1976.

992 Shardt, N., Isenrich, F. N., Waser, B., Marcolli, C., Kanji, Z. A., deMello, A. J., and Lohmann,
993 U.: Homogeneous freezing of water droplets for different volumes and cooling rates, Phys.
994 Chem. Chem. Phys., 24, 28213–28221, <https://doi.org/10.1039/D2CP03896J>, 2022.

995 Tabari, H.: Climate change impact on flood and extreme precipitation increases with water
996 availability, Sci. Rep., 10, 13768, <https://doi.org/10.1038/s41598-020-70816-2>, 2020.

997 Tarn, M. D., Sikora, S. N. F., Porter, G. C. E., Shim, J., and Murray, B. J.: Homogeneous
998 Freezing of Water Using Microfluidics, Micromachines, 12, 223,
999 <https://doi.org/10.3390/mi12020223>, 2021.

1000 Toll, V., Rahu, J., Keernik, H., Trofimov, H., Voormansik, T., Manshausen, P., Hung, E.,
1001 Michelson, D., Christensen, M. W., Post, P., Junninen, H., Murray, B. J., Lohmann, U., Watson-
1002 Parris, D., Stier, P., Donaldson, N., Storelvmo, T., Kulmala, M., and Bellouin, N.: Glaciation
1003 of liquid clouds, snowfall, and reduced cloud cover at industrial aerosol hot spots, Science, 386,
1004 756–762, <https://doi.org/10.1126/science.adl0303>, 2024.

1005 Trofimov, H., Post, P., Gryspeerdt, E., and Toll, V.: Meteorological Conditions Favorable for
1006 Strong Anthropogenic Aerosol Impacts on Clouds, J. Geophys. Res. Atmospheres, 127,
1007 e2021JD035871, <https://doi.org/10.1029/2021JD035871>, 2022.

1008 Vali, G.: Ice Nucleation — a review, in: Nucleation and Atmospheric Aerosols 1996, Elsevier,
1009 271–279, <https://doi.org/10.1016/B978-008042030-1/50066-4>, 1996.

1010 Vega, E., Reyes, E., Ruiz, H., García, J., Sánchez, G., Martínez-Villa, G., González, U., Chow,
1011 J. C., and Watson, J. G.: Analysis of PM_{2.5} and PM₁₀ in the Atmosphere of Mexico City during

1012 [2000-2002, J. Air Waste Manag. Assoc., 54, 786–798,](https://doi.org/10.1080/10473289.2004.10470952)
1013 [https://doi.org/10.1080/10473289.2004.10470952, 2004.](https://doi.org/10.1080/10473289.2004.10470952)

1014 [Wex, H., Augustin-Bauditz, S., Boose, Y., Budke, C., Curtius, J., Diehl, K., Dreyer, A., Frank,](https://doi.org/10.5194/acp-15-1463-2015)
1015 [F., Hartmann, S., Hiranuma, N., Jantsch, E., Kanji, Z. A., Kiselev, A., Koop, T., Möhler, O.,](https://doi.org/10.5194/acp-15-1463-2015)
1016 [Niedermeier, D., Nillius, B., Rösch, M., Rose, D., Schmidt, C., Steinke, I., and Stratmann, F.:](https://doi.org/10.5194/acp-15-1463-2015)
1017 [Intercomparing different devices for the investigation of ice nucleating particles using Snomax[®]](https://doi.org/10.5194/acp-15-1463-2015)
1018 [as test substance, Atmospheric Chem. Phys., 15, 1463–1485, https://doi.org/10.5194/acp-15-](https://doi.org/10.5194/acp-15-1463-2015)
1019 [1463-2015, 2015.](https://doi.org/10.5194/acp-15-1463-2015)

1020 [Zhao, B., Wang, Y., Gu, Y., Liou, K.-N., Jiang, J. H., Fan, J., Liu, X., Huang, L., and Yung, Y.](https://doi.org/10.1038/s41561-019-0389-4)
1021 [L.: Ice nucleation by aerosols from anthropogenic pollution, Nat. Geosci., 12, 602–607,](https://doi.org/10.1038/s41561-019-0389-4)
1022 [https://doi.org/10.1038/s41561-019-0389-4, 2019.](https://doi.org/10.1038/s41561-019-0389-4)

1023 [Zhu, Z., Peng, C., Li, X., Zhang, R., Dai, X., Jiang, B., and Chen, J.: Remote Sensing-Based](https://doi.org/10.3390/w16162345)
1024 [Analysis of Precipitation Events: Spatiotemporal Characterization across China, Water, 16,](https://doi.org/10.3390/w16162345)
1025 [2345, https://doi.org/10.3390/w16162345, 2024.](https://doi.org/10.3390/w16162345)

1026 [Agresti, A. and Coull, B. A.: Approximate is Better than “Exact” for Interval Estimation of](https://doi.org/10.1080/00031305.1998.10480550)
1027 [Binomial Proportions, Am. Stat., 52, 119–126,](https://doi.org/10.1080/00031305.1998.10480550)
1028 [https://doi.org/10.1080/00031305.1998.10480550, 1998.](https://doi.org/10.1080/00031305.1998.10480550)

1029 [Aiken, A. C., Salcedo, D., Cubison, M. J., Huffman, J. A., DeCarlo, P. F., Ulbrich, I. M.,](https://doi.org/10.5194/acp-9-6633-2009)
1030 [Docherty, K. S., Sueper, D., Kimmel, J. R., Worsnop, D. R., Trimborn, A., Northway, M.,](https://doi.org/10.5194/acp-9-6633-2009)
1031 [Stone, E. A., Schauer, J. J., Volkamer, R. M., Fortner, E., de Foy, B., Wang, J., Laskin, A.,](https://doi.org/10.5194/acp-9-6633-2009)
1032 [Shutthanandan, V., Zheng, J., Zhang, R., Gaffney, J., Marley, N. A., Paredes-Miranda, G.,](https://doi.org/10.5194/acp-9-6633-2009)
1033 [Arnott, W. P., Molina, L. T., Sosa, G., and Jimenez, J. L.: Mexico City aerosol analysis during](https://doi.org/10.5194/acp-9-6633-2009)
1034 [MILAGRO using high resolution aerosol mass spectrometry at the urban supersite \(T0\) Part](https://doi.org/10.5194/acp-9-6633-2009)
1035 [I: Fine particle composition and organic source apportionment, Atmos Chem Phys,](https://doi.org/10.5194/acp-9-6633-2009)
1036 [https://doi.org/10.5194/acp-9-6633-2009, 2009.](https://doi.org/10.5194/acp-9-6633-2009)

1037 [Aldape, F., Flores M., J., Diaz, R. V., Morales, J. R., Cahill, T. A., and Saravia, L.: Seasonal](https://doi.org/10.1142/S012908359100024X)
1038 [study of the composition of atmospheric aerosols in Mexico City, Int. J. PIXE, 01, 355–371,](https://doi.org/10.1142/S012908359100024X)
1039 [https://doi.org/10.1142/S012908359100024X, 1991.](https://doi.org/10.1142/S012908359100024X)

1040 [Amador Muñoz, O., Villalobos Pietrini, R., Miranda, J., and Vera Avila, L. E.: Organic](https://doi.org/10.1016/j.scitotenv.2010.11.026)
1041 [compounds of PM_{2.5} in Mexico Valley: Spatial and temporal patterns, behavior and sources,](https://doi.org/10.1016/j.scitotenv.2010.11.026)
1042 [Sci. Total Environ., 409, 1453–1465, https://doi.org/10.1016/j.scitotenv.2010.11.026, 2011.](https://doi.org/10.1016/j.scitotenv.2010.11.026)

1043 [Amador Muñoz, O., Bazán-Torija, S., Villa-Ferreira, S. A., Villalobos Pietrini, R., Bravo-](https://doi.org/10.1016/j.atmosres.2012.10.003)
1044 [Cabrera, J. L., Munive Colín, Z., Hernández Mena, L., Saldarriaga Noreña, H., and Murillo-](https://doi.org/10.1016/j.atmosres.2012.10.003)
1045 [Tovar, M. A.: Opposing seasonal trends for polycyclic aromatic hydrocarbons and PM₁₀:](https://doi.org/10.1016/j.atmosres.2012.10.003)
1046 [Health risk and sources in southwest Mexico City, Atmospheric Res., 122, 199–212,](https://doi.org/10.1016/j.atmosres.2012.10.003)
1047 [https://doi.org/10.1016/j.atmosres.2012.10.003, 2013.](https://doi.org/10.1016/j.atmosres.2012.10.003)

1048 [Amador Muñoz, O., Misztal, P. K., Weber, R., Worton, D. R., Zhang, H., Drozd, G., and](https://doi.org/10.5194/amt-9-5315-2016)
1049 [Goldstein, A. H.: Sensitive detection of *n*-alkanes using a mixed ionization mode proton-](https://doi.org/10.5194/amt-9-5315-2016)
1050 [transfer reaction mass spectrometer, Atmospheric Meas. Tech., 9, 5315–5329,](https://doi.org/10.5194/amt-9-5315-2016)
1051 [https://doi.org/10.5194/amt-9-5315-2016, 2016.](https://doi.org/10.5194/amt-9-5315-2016)

1052 Behzadi, F., Wasti, A., Haque Rahat, S., Tracy, J. N., and Ray, P. A.: Analysis of the climate
1053 change signal in Mexico City given disagreeing data sources and scattered projections, *J.*
1054 *Hydrol. Reg. Stud.*, *27*, 100662, <https://doi.org/10.1016/j.ejrh.2019.100662>, 2020.

1055 Bi, K., McMeeking, G. R., Ding, D. P., Levin, E. J. T., DeMott, P. J., Zhao, D. L., Wang, F.,
1056 Liu, Q., Tian, P., Ma, X. C., Chen, Y. B., Huang, M. Y., Zhang, H. L., Gordon, T. D., and Chen,
1057 P.: Measurements of Ice Nucleating Particles in Beijing, China, *J. Geophys. Res. Atmospheres*,
1058 *124*, 8065–8075, <https://doi.org/10.1029/2019JD030609>, 2019.

1059 Burrows, S. M., McCluskey, C. S., Cornwell, G., Steinke, I., Zhang, K., Zhao, B., Zawadowicz,
1060 M., Raman, A., Kulkarni, G., China, S., Zelenyuk, A., and DeMott, P. J.: Ice Nucleating
1061 Particles That Impact Clouds and Climate: Observational and Modeling Research Needs, *Rev.*
1062 *Geophys.*, *60*, e2021RG000745, <https://doi.org/10.1029/2021RG000745>, 2022.

1063 Cabrera-Segoviano, D., Pereira, D. L., Rodriguez, C., Raga, G. B., Miranda, J., Alvarez-Ospina,
1064 H., and Ladino, L. A.: Inter-annual variability of ice nucleating particles in Mexico City, *Atmos.*
1065 *Environ.*, *273*, 118964, <https://doi.org/10.1016/j.atmosenv.2022.118964>, 2022.

1066 Carabali, G., Villanueva-Macias, J., Ladino, L. A., Álvarez-Ospina, H., Raga, G. B., Andraca-
1067 Ayala, G., Miranda, J., Grutter, M., Silva, Ma. M., and Riveros-Rosas, D.: Characterization of
1068 aerosol particles during a high pollution episode over Mexico City, *Sci. Rep.*, *11*, 22533,
1069 <https://doi.org/10.1038/s41598-021-01873-4>, 2021.

1070 Castro-Romero, T., Peralta, O., Prieto, C., Santiago, N., Alvarez-Ospina, H., García-Martínez,
1071 R., Saavedra Rosado, I., Espinosa Fuentes, M. D. L. L., Hernández, E., Miranda, J., Gómez, V.,
1072 Solís, C., Salcedo, D., Torres Jardón, R., Martínez-Arroyo, A., Ortíz-Álvarez, A., Ruíz-
1073 Suárez, G., and Ortiz, E.: Characterization of PM_{2.5} during ACU15 campaign in Mexico City,
1074 *Geofísica Int.*, *63*, 1225–1238, <https://doi.org/10.22201/igeof.2954436xe.2024.63.4.1745>,
1075 2024.

1076 Celada-Murillo, A. T., Carreón-Sierra, S., Salcido, A., Castro, T., Peralta, O., and Georgiadis,
1077 T.: Main Characteristics of Mexico City Local Wind Events during the MILAGRO 2006
1078 Campaign within a Meso- β Scale Lattice Wind Modeling Approach, *ISRN Meteorol.*, 2013,
1079 1–14, <https://doi.org/10.1155/2013/605210>, 2013.

1080 Chen, J., Wu, Z., Augustin-Bauditz, S., Grawe, S., Hartmann, M., Pei, X., Liu, Z., Ji, D., and
1081 Wex, H.: Ice-nucleating particle concentrations unaffected by urban air pollution in Beijing,
1082 China, *Atmospheric Chem. Phys.*, *18*, 3523–3539, <https://doi.org/10.5194/acp-18-3523-2018>,
1083 2018.

1084 Chen, J., Wu, Z., Gong, X., Qiu, Y., Chen, S., Zeng, L., and Hu, M.: Anthropogenic Dust as a
1085 Significant Source of Ice Nucleating Particles in the Urban Environment, *Earths Future*, *12*,
1086 e2023EF003738, <https://doi.org/10.1029/2023EF003738>, 2024.

1087 Cooke, M. E., Waters, C. M., Asare, J. Y., Mirrielees, J. A., Holen, A. L., Frauenheim, M. P.,
1088 Zhang, Z., Gold, A., Pratt, K. A., Surratt, J. D., Ladino, L. A., and Ault, A. P.: Atmospheric
1089 Aerosol Sulfur Distribution and Speciation in Mexico City: Sulfate, Organosulfates, and
1090 Isoprene-Derived Secondary Organic Aerosol from Low NO Pathways, *ACS EST Air*, *1*, 1037–
1091 1052, <https://doi.org/10.1021/acsestair.4c00048>, 2024.

1092 Córdoba, F., Ramírez-Romero, C., Cabrera, D., Raga, G. B., Miranda, J., Alvarez-Ospina, H.,
1093 Rosas, D., Figueroa, B., Kim, J. S., Yakobi Hancock, J., Amador, T., Gutierrez, W., García,

1094 M., Bertram, A. K., Baumgardner, D., and Ladino, L. A.: Measurement report: Ice nucleating
1095 abilities of biomass burning, African dust, and sea spray aerosol particles over the Yucatán
1096 Peninsula, *Atmospheric Chem. Phys.*, 21, 4453–4470, [https://doi.org/10.5194/acp-21-4453-](https://doi.org/10.5194/acp-21-4453-2021)
1097 [2021](https://doi.org/10.5194/acp-21-4453-2021), 2021.

1098 Doran, J. C., Arnott, W. P., Barnard, J. C., Cary, R., Coulter, R., Fast, J. D., Kassianov, E. I.,
1099 Kleinman, L., Laulainen, N. S., Martin, T., Paredes Miranda, G., Pekour, M. S., Shaw, W. J.,
1100 Smith, D. F., and Springston, S. R.: The T1–T2 study: evolution of aerosol properties downwind
1101 of Mexico City, *Atmospheric Chem. Phys. Discuss.*, 6 (6), 12967–12999.,
1102 <https://doi.org/10.5194/acp-7-1585-2007>, 2007.

1103 Draxler, R.R., R., G. D.: HYSPLIT (HYbrid Single Particle Lagrangian Integrated Trajectory)
1104 Model, 2010.

1105 Edgerton, S. A., Bian, X., Doran, J. C., Fast, J. D., Hubbe, J. M., Malone, E. L., Shaw, W. J.,
1106 Whiteman, C. D., Zhong, S., Arriaga, J. L., Ortiz, E., Ruiz, M., Sosa, G., Vega, E., Limon, T.,
1107 Guzman, F., Archuleta, J., Bossert, J. E., Elliot, S. M., Lee, J. T., McNair, L. A., Chow, J. C.,
1108 Watson, J. G., Coulter, R. L., Doskey, P. V., Gaffney, J. S., Marley, N. A., Neff, W., and Petty,
1109 R.: Particulate Air Pollution in Mexico City: A Collaborative Research Project, *J. Air Waste*
1110 *Manag. Assoc.*, 49, 1221–1229, <https://doi.org/10.1080/10473289.1999.10463915>, 1999.

1111 Espinosa, A., Miranda, J., and Pineda, J.C: Uncertainty evaluation in correlated quantities:
1112 application to elemental analysis of atmospheric aerosols, *Rev. Mex. Física*, 56 (1), 134–140,
1113 2010.

1114 Espinosa, A. A., Reyes-Herrera, J., Miranda, J., Mercado, F., Veytia, M. A., Cuautle, M., and
1115 Cruz, J. I.: Development of an X-ray fluorescence spectrometer for environmental science
1116 applications, *Instrum. Sci. Technol.*, 40, 603–617,
1117 <https://doi.org/10.1080/10739149.2012.693560>, 2012.

1118 Gimeno, L., Sorí, R., Vázquez, M., Stojanovic, M., Algarra, I., Eiras-Barca, J., Gimeno-Sotelo,
1119 L., and Nieto, R.: Extreme precipitation events, *WIREs Water*, 9, e1611,
1120 <https://doi.org/10.1002/wat2.1611>, 2022.

1121 Hasenkopf, C. A., Veghte, D. P., Schill, G. P., Lodoysamba, S., Freedman, M. A., and Tolbert,
1122 M. A.: Ice nucleation, shape, and composition of aerosol particles in one of the most polluted
1123 cities in the world: Ulaanbaatar, Mongolia, *Atmos. Environ.*, 139, 222–229,
1124 <https://doi.org/10.1016/j.atmosenv.2016.05.037>, 2016.

1125 Hernández-López, A. E., Miranda-Martín-Del-Campo, J., Mugica-Álvarez, V., Hernández-
1126 Valle, B. L., Mejía-Ponce, L. V., Pineda-Santamaría, J. C., Reynoso-Cruces, S., Mendoza-
1127 Flores, J. A., and Rozanes-Valenzuela, D.: A study of PM_{2.5} elemental composition in
1128 southwest Mexico City and development of receptor models with positive matrix factorization,
1129 *Rev. Int. Contam. Ambient.*, <https://doi.org/10.20937/RICA.54066>, 2020.

1130 Hernández-López, A. E., Santos-Medina, G. L., Morton-Bermea, O., Hernández-Álvarez, E.,
1131 Villalobos-Pietrini, R., and Amador-Muñoz, O.: Chemical speciation of organic compounds
1132 and elemental compositions of PM_{2.5} in Mexico City: Spatial-seasonal distribution, emission
1133 sources, and formation processes, *Atmospheric Res.*, 292, 106868,
1134 <https://doi.org/10.1016/j.atmosres.2023.106868>, 2023.

1135 Heymsfield, A. J., Schmitt, C., Chen, C. C. J., Bansemer, A., Gettelman, A., Field, P. R., and
1136 Liu, C.: Contributions of the Liquid and Ice Phases to Global Surface Precipitation:
1137 Observations and Global Climate Modeling, *J. Atmospheric Sci.*, *77*, 2629–2648,
1138 <https://doi.org/10.1175/JAS-D-19-0352.1>, 2020.

1139 Hoose, C. and Möhler, O.: Heterogeneous ice nucleation on atmospheric aerosols: a review of
1140 results from laboratory experiments, *Atmospheric Chem. Phys.*, *12*, 9817–9854,
1141 <https://doi.org/10.5194/acp-12-9817-2012>, 2012.

1142 Hoose, C., Kristjánsson, J. E., and Burrows, S. M.: How important is biological ice nucleation
1143 in clouds on a global scale?, *Environ. Res. Lett.*, *5*, 024009, <https://doi.org/10.1088/1748-9326/5/2/024009>, 2010.

1145 Houze, R. A.: *Cloud dynamics*, Second edition., Academic Press, Oxford, England, 2014.

1146 Hurtado, L., Rodríguez, G., López, J., Castillo, J. E., Molina, L., Zavala, M., and Quintana, P.
1147 J. E.: Characterization of atmospheric bioaerosols at 9 sites in Tijuana, Mexico, *Atmos.
1148 Environ.*, *96*, 430–436, <https://doi.org/10.1016/j.atmosenv.2014.07.018>, 2014.

1149 Población: <https://www.inegi.org.mx/temas/estructura/>, last access: 10 October 2025.

1150 Jahl, L. G., Brubaker, T. A., Polen, M. J., Jahn, L. G., Cain, K. P., Bowers, B. B., Fahy, W. D.,
1151 Graves, S., and Sullivan, R. C.: Atmospheric aging enhances the ice nucleation ability of
1152 biomass-burning aerosol, *Sci. Adv.*, *7*, <https://doi.org/10.1126/sciadv.abd3440>, 2021.

1153 Jahn, L. G., Polen, M. J., Jahl, L. G., Brubaker, T. A., Somers, J., and Sullivan, R. C.: Biomass
1154 combustion produces ice-active minerals in biomass-burning aerosol and bottom ash, *Proc.
1155 Natl. Acad. Sci.*, *117*, 21928–21937, <https://doi.org/10.1073/pnas.1922128117>, 2020.

1156 Jáuregui, E.: *El clima de la Ciudad de México*, 1. ed., Instituto de Geografía, UNAM: Plaza y
1157 Valdés Editores, México, D.F., 131 pp., 2000.

1158 Kanji, Z. A., Ladino, L. A., Wex, H., Boose, Y., Burkert-Kohn, M., Cziezo, D. J., and Krämer,
1159 M.: Overview of Ice Nucleating Particles, *Meteorol. Monogr.*, *58*, 1.1–1.33,
1160 <https://doi.org/10.1175/AMSMONOGRAPHIS-D-16-0006.1>, 2017.

1161 Knopf, D. A., Wang, B., Laskin, A., Moffet, R. C., and Gilles, M. K.: Heterogeneous nucleation
1162 of ice on anthropogenic organic particles collected in Mexico City, *Geophys. Res. Lett.*, *37*,
1163 2010GL043362, <https://doi.org/10.1029/2010GL043362>, 2010.

1164 Knopf, D. A., Alpert, P. A., Wang, B., and Aller, J. Y.: Stimulation of ice nucleation by marine
1165 diatoms, *Nat. Geosci.*, *4*, 88–90, <https://doi.org/10.1038/ngeo1037>, 2011.

1166 Kunert, A. T., Pöhlker, M. L., Tang, K., Krevert, C. S., Wieder, C., Speth, K. R., Hanson, L.
1167 E., Morris, C. E., Schmale Iii, D. G., Pöschl, U., and Fröhlich Nowoisky, J.: Macromolecular
1168 fungal ice nuclei in *Fusarium*: effects of physical and chemical processing, *Biogeosciences*,
1169 *16*, 4647–4659, <https://doi.org/10.5194/bg-16-4647-2019>, 2019.

1170 Ladino, L. A., Raga, G. B., and Baumgardner, D.: On particle-bound polycyclic aromatic
1171 hydrocarbons (PPAH) and links to gaseous emissions in Mexico City, *Atmos. Environ.*, *194*,
1172 31–40, <https://doi.org/10.1016/j.atmosenv.2018.09.022>, 2018.

1173 Lezama, J. L. and Vargas, V. I.: Las fuerzas rectoras de la contaminación del aire en la Ciudad
1174 de México, MIT Integr. Program Urban Reg. Glob. Air Pollut. Rep. NO8 Camb. MA, 2000.

1175 Li, C., Zwiers, F., Zhang, X., Chen, G., Lu, J., Li, G., Norris, J., Tan, Y., Sun, Y., and Liu, M.:
1176 Larger Increases in More Extreme Local Precipitation Events as Climate Warms, *Geophys.*
1177 *Res. Lett.*, 46, 6885–6891, <https://doi.org/10.1029/2019GL082908>, 2019.

1178 Li, M., Qi, J., Zhang, H., Huang, S., Li, L., and Gao, D.: Concentration and size distribution of
1179 bioaerosols in an outdoor environment in the Qingdao coastal region, *Sci. Total Environ.*, 409,
1180 3812–3819, <https://doi.org/10.1016/j.scitotenv.2011.06.001>, 2011.

1181 Mason, R. H., Chou, C., McCluskey, C. S., Levin, E. J. T., Schiller, C. L., Hill, T. C. J.,
1182 Huffman, J. A., DeMott, P. J., and Bertram, A. K.: The micro-orifice uniform deposit impactor-
1183 droplet-freezing technique (MOUDI-DFT) for measuring concentrations of ice-nucleating
1184 particles as a function of size: improvements and initial validation, *Atmospheric Meas. Tech.*,
1185 8, 2449–2462, <https://doi.org/10.5194/amt-8-2449-2015>, 2015.

1186 Mason, R. H., Si, M., Chou, C., Irish, V. E., Dickie, R., Elizondo, P., Wong, R., Brintnell, M.,
1187 Elsasser, M., Lassar, W. M., Pierce, K. M., Leaitch, W. R., MacDonald, A. M., Platt, A., Toom-
1188 Saunty, D., Sarda-Estève, R., Schiller, C. L., Suski, K. J., Hill, T. C. J., Abbatt, J. P. D.,
1189 Huffman, J. A., DeMott, P. J., and Bertram, A. K.: Size-resolved measurements of ice-
1190 nucleating particles at six locations in North America and one in Europe, *Atmospheric Chem.*
1191 *Phys.*, 16, 1637–1651, <https://doi.org/10.5194/acp-16-1637-2016>, 2016.

1192 Melchum, A., Córdoba, F., Salinas, E., Martínez, L., Campos, G., Rosas, I., Garcia-Mendoza,
1193 E., Olivos-Ortiz, A., Raga, G. B., Pizano, B., Silva, Ma. M., and Ladino, L. A.: Maritime and
1194 continental microorganisms collected in Mexico: An investigation of their ice-nucleating
1195 abilities, *Atmospheric Res.*, 293, 106893, <https://doi.org/10.1016/j.atmosres.2023.106893>,
1196 2023.

1197 Met Office, 2023, "Microclimates," National Meteorological Library and Archive Factsheet 14,
1198 [https://www.metoffice.gov.uk/binaries/content/assets/metofficegovuk/pdf/research/library-](https://www.metoffice.gov.uk/binaries/content/assets/metofficegovuk/pdf/research/library-and-archive/library/publications/factsheets/factsheet_14_microclimates_2023.pdf)
1199 [and-archive/library/publications/factsheets/factsheet_14_microclimates_2023.pdf](https://www.metoffice.gov.uk/binaries/content/assets/metofficegovuk/pdf/research/library-and-archive/library/publications/factsheets/factsheet_14_microclimates_2023.pdf), last access:
1200 17 February 2026.

1201 Molina, H., Yang, Y., Ruch, T., Kim, J. W., Mortensen, P., Otto, T., Nalli, A., Tang, Q. Q.,
1202 Lane, M. D., Chaerkady, R., and Pandey, A.: Temporal Profiling of the Adipocyte Proteome
1203 during Differentiation Using a Five-Plex SILAC-Based Strategy, *J. Proteome Res.*, 8, 48–58,
1204 <https://doi.org/10.1021/pr800650r>, 2009.

1205 Molina, L. T., Madronich, S., Gaffney, J. S., Apel, E., De Foy, B., Fast, J., Ferrare, R., Herndon,
1206 S., Jimenez, J. L., Lamb, B., Osornio-Vargas, A. R., Russell, P., Schauer, J. J., Stevens, P. S.,
1207 Volkamer, R., and Zavala, M.: An overview of the MILAGRO 2006 Campaign: Mexico City
1208 emissions and their transport and transformation, *Atmospheric Chem. Phys.*, 10, 8697–8760,
1209 <https://doi.org/10.5194/acp-10-8697-2010>, 2010.

1210 Molina, M. J. and Molina, L. T.: Megacities and Atmospheric Pollution, *J. Air Waste Manag.*
1211 *Assoc.*, 54, 644–680, <https://doi.org/10.1080/10473289.2004.10470936>, 2004.

1212 Moreno, T., Querol, X., Pey, J., Minguillón, M. C., Pérez, N., Alastuey, A., Bernabé, R. M.,
1213 Blanco, S., Cárdenas, B., Eichinger, W., Saleido, A., and Gibbons, W.: Spatial and temporal

1214 variations in inhalable CuZnPb aerosols within the Mexico City pollution plume, *J. Environ.*
1215 *Monit.*, 10, 370, <https://doi.org/10.1039/b716507b>, 2008.

1216 Mülmenstädt, J., Sourdeval, O., Delanoë, J., and Quaas, J.: Frequency of occurrence of rain
1217 from liquid, mixed, and ice phase clouds derived from A-Train satellite retrievals, *Geophys.*
1218 *Res. Lett.*, 42, 6502–6509, <https://doi.org/10.1002/2015GL064604>, 2015.

1219 Ohneiser, K., Seifert, P., Schimmel, W., Senf, F., Gaudek, T., Radenz, M., Teisseire, A.,
1220 Ettrichrätz, V., Vogl, T., Mahernndl, N., Pfeifer, N., Henneberger, J., Miller, A. J., Omanovic,
1221 N., Fuchs, C., Zhang, H., Ramelli, F., Spirig, R., Kötsche, A., Kalesse-Los, H., Maahn, M.,
1222 Corden, H., Berne, A., Hajipour, M., Griesche, H., Hofer, J., Engelmann, R., Skupin, A.,
1223 Ansmann, A., and Baars, H.: Impact of seeder-feeder cloud interaction on precipitation
1224 formation: a case study based on extensive remote sensing, in situ and model data, *Atmospheric*
1225 *Chem. Phys.*, 25, 17363–17386, <https://doi.org/10.5194/acp-25-17363-2025>, 2025.

1226 Pereira, D. L., Silva, M. M., García, R., Raga, G. B., Alvarez-Ospina, H., Carabali, G., Rosas,
1227 I., Martínez, L., Salinas, E., Hidalgo-Bonilla, S., and Ladino, L. A.: Characterization of ice
1228 nucleating particles in rainwater, cloud water, and aerosol samples at two different tropical
1229 latitudes, *Atmospheric Res.*, 250, 105356, <https://doi.org/10.1016/j.atmosres.2020.105356>,
1230 2021.

1231 Pinto, D. M., Blande, J. D., Souza, S. R., Nerg, A. M., and Holopainen, J. K.: Plant Volatile
1232 Organic Compounds (VOCs) in Ozone (O₃) Polluted Atmospheres: The Ecological Effects, *J.*
1233 *Chem. Ecol.*, 36, 22–34, <https://doi.org/10.1007/s10886-009-9732-3>, 2010.

1234 Prenni, A. J., DeMott, P. J., Sullivan, A. P., Sullivan, R. C., Kreidenweis, S. M., and Rogers,
1235 D. C.: Biomass burning as a potential source for atmospheric ice nuclei: Western wildfires and
1236 prescribed burns, *Geophys. Res. Lett.*, 39, <https://doi.org/10.1029/2012gl051915>, 2012.

1237 Purdy, J. C., Austin, G. L., Seed, A. W., and Cluckie, I. D.: Radar evidence of orographic
1238 enhancement due to the seeder-feeder mechanism, *Meteorol. Appl.*, 12, 199–206,
1239 <https://doi.org/10.1017/S1350482705001672>, 2005.

1240 Querol, X., Pey, J., Minguillón, M. C., Pérez, N., Alastuey, A., Viana, M., Moreno, T., Bernabé,
1241 R. M., Blanco, S., Cárdenas, B., Vega, E., Sosa, G., Escalona, S., Ruiz, H., and Artíñano, B.:
1242 PM speciation and sources in Mexico during the MILAGRO 2006 Campaign, *Atmospheric*
1243 *Chem. Phys.*, 8, 111–128, <https://doi.org/10.5194/acp-8-111-2008>, 2008.

1244 Querol, X., Tobías, A., Pérez, N., Karanasiou, A., Amato, F., Stafoggia, M., Pérez-García-
1245 Pando, C., Ginoux, P., Forastiere, F., Gumy, S., Mudu, P., and Alastuey, A.: Monitoring the
1246 impact of desert dust outbreaks for air quality for health studies, *Environ. Int.*, 130, 104867,
1247 <https://doi.org/10.1016/j.envint.2019.05.061>, 2019.

1248 Raga, G. B., Ladino, L. A., Baumgardner, D., Ramirez-Romero, C., Córdoba, F., Alvarez-
1249 Ospina, H., Rosas, D., Amador, T., Miranda, J., Rosas, I., Jaramillo, A., Yakobi-Hancock, J.,
1250 Kim, J. S., Martínez, L., Salinas, E., and Figueroa, B.: ADABBOY: African Dust And Biomass
1251 Burning Over Yucatan, *Bull. Am. Meteorol. Soc.*, 102, E1543–E1556,
1252 <https://doi.org/10.1175/BAMS-D-20-0172.1>, 2021.

1253 Reynoso-Cruces, S., Miranda-Martín-Del-Campo, J., and Pineda-Santamaría, J. C.: Elemental
1254 composition of PM₁₀ in indoor environments of a scientific research institution and risk

1255 assessment, *Environ. Pollut. Bioavail.*, **35**, 2232108,
1256 <https://doi.org/10.1080/26395940.2023.2232108>, 2023.

1257 Riojas-Rodríguez, H., Álamo-Hernández, U., Texcalac-Sangrador, J. L., and Romieu, I.: Health
1258 impact assessment of decreases in PM10 and ozone concentrations in the Mexico City
1259 Metropolitan Area. A basis for a new air quality management program, *Salud Pública México*,
1260 **56**, 579, <https://doi.org/10.21149/spm.v56i6.7384>, 2014.

1261 Ríos, B. and Raga, G. B.: Spatio-temporal distribution of burned areas by ecoregions in Mexico
1262 and Central America, *Int. J. Remote Sens.*, **39**, 949–970,
1263 <https://doi.org/10.1080/01431161.2017.1392641>, 2018.

1264 Rodríguez-Gómez, C.: Variabilidad de los núcleos de glaciación en la capa límite y la tropósfera
1265 libre en Altzomoni, y su influencia en la formación de nubes mixtas, Universidad Nacional
1266 Autónoma de México, México, CDMX, 128 pp., 2021.

1267 Rodríguez-Gómez, C., Ramírez-Romero, C., Córdoba, F., Raga, G. B., Salinas, E., Martínez,
1268 L., Rosas, I., Quintana, E. T., Maldonado, L. A., Rosas, D., Amador, T., Álvarez, H., and
1269 Ladino, L. A.: Characterization of culturable airborne microorganisms in the Yucatan
1270 Peninsula, *Atmos. Environ.*, **223**, 117183, <https://doi.org/10.1016/j.atmosenv.2019.117183>,
1271 2020.

1272 Rogers, R. R. and Yau, M. K.: *A short course in cloud physics*, Third edition., Butterworth-
1273 Heinemann, Burlington, Massachusetts, 1 pp., 1996.

1274 Rosas, D., Silva, M. M., Figueroa, B., Morton-Bermea, O., Miranda, J., Álvarez, H., Puig, T.,
1275 Morales, J., Uuh, J., Hernández-Alvarez, E., Novelo, S., Olivares, J., Salcedo, D., Rosas, I.,
1276 Ponce, C., Raga, G. B., and Ladino, L. A.: African dust particles over the western Caribbean:
1277 Chemical characterization, *Atmos. Environ.*, **347**, 121095,
1278 <https://doi.org/10.1016/j.atmosenv.2025.121095>, 2025.

1279 Russy-Velandia, L., Ramírez, O., Barrera, J., Mendoza-Téllez, S., Álvarez, H., Patiño, M. C.,
1280 and Ladino, L. A.: Approach to culturable bioaerosols and their environmental drivers at a
1281 border site in the northwestern Amazon, *Atmospheric Environ.*, **X**, **27**, 100362,
1282 <https://doi.org/10.1016/j.aeaoa.2025.100362>, 2025.

1283 Salcido, A., Carreón-Sierra, S., Georgiadis, T., Celada-Murillo, A. T., and Castro, T.: Lattice
1284 Wind Description and Characterization of Mexico City Local Wind Events in the 2001–2006
1285 Period, *Climate*, **3**, 542–562, <https://doi.org/10.3390/cli3030542>, 2015.

1286 Schnell, R. C. and Vali, G.: Biogenic Ice Nuclei: Part I. Terrestrial and Marine Sources, *J.*
1287 *Atmospheric Sci.*, **33**, 1554–1564, [https://doi.org/10.1175/1520-0469\(1976\)033%253C1554:BINPIT%253E2.0.CO;2](https://doi.org/10.1175/1520-0469(1976)033%253C1554:BINPIT%253E2.0.CO;2), 1976.

1289 Shardt, N., Isenrich, F. N., Waser, B., Marcolli, C., Kanji, Z. A., deMello, A. J., and Lohmann,
1290 U.: Homogeneous freezing of water droplets for different volumes and cooling rates, *Phys.*
1291 *Chem. Chem. Phys.*, **24**, 28213–28221, <https://doi.org/10.1039/D2CP03896J>, 2022.

1292 Tabari, H.: Climate change impact on flood and extreme precipitation increases with water
1293 availability, *Sci. Rep.*, **10**, 13768, <https://doi.org/10.1038/s41598-020-70816-2>, 2020.

1294 Tarn, M. D., Sikora, S. N. F., Porter, G. C. E., Shim, J., and Murray, B. J.: Homogeneous
1295 Freezing of Water Using Microfluidics, *Micromachines*, 12, 223,
1296 <https://doi.org/10.3390/mi12020223>, 2021.

1297 Toll, V., Rahu, J., Keernik, H., Trofimov, H., Voormansik, T., Manshausen, P., Hung, E.,
1298 Michelson, D., Christensen, M. W., Post, P., Junninen, H., Murray, B. J., Lohmann, U., Watson-
1299 Parris, D., Stier, P., Donaldson, N., Storelvmo, T., Kulmala, M., and Bellouin, N.: Glaciation
1300 of liquid clouds, snowfall, and reduced cloud cover at industrial aerosol hot spots, *Science*, 386,
1301 756–762, <https://doi.org/10.1126/science.adl0303>, 2024.

1302 Trofimov, H., Post, P., Gryspeerdt, E., and Toll, V.: Meteorological Conditions Favorable for
1303 Strong Anthropogenic Aerosol Impacts on Clouds, *J. Geophys. Res. Atmospheres*, 127,
1304 e2021JD035871, <https://doi.org/10.1029/2021JD035871>, 2022.

1305 Vali, G.: Ice Nucleation—a review, in: *Nucleation and Atmospheric Aerosols 1996*, Elsevier,
1306 271–279, <https://doi.org/10.1016/B978-008042030-1/50066-4>, 1996.

1307 Vega, E., Reyes, E., Ruiz, H., García, J., Sánchez, G., Martínez-Villa, G., González, U., Chow,
1308 J. C., and Watson, J. G.: Analysis of PM_{2.5} and PM₁₀ in the Atmosphere of Mexico City during
1309 2000–2002, *J. Air Waste Manag. Assoc.*, 54, 786–798,
1310 <https://doi.org/10.1080/10473289.2004.10470952>, 2004.

1311 Wex, H., Augustin-Bauditz, S., Boose, Y., Budke, C., Curtius, J., Diehl, K., Dreyer, A., Frank,
1312 F., Hartmann, S., Hiranuma, N., Jantsch, E., Kanji, Z. A., Kiselev, A., Koop, T., Möhler, O.,
1313 Niedermeier, D., Nillius, B., Rösch, M., Rose, D., Schmidt, C., Steinke, I., and Stratmann, F.:
1314 Intercomparing different devices for the investigation of ice nucleating particles using Snomax[®]
1315 as test substance, *Atmospheric Chem. Phys.*, 15, 1463–1485, [https://doi.org/10.5194/acp-15-](https://doi.org/10.5194/acp-15-1463-2015)
1316 1463–2015, 2015.

1317 Zhao, B., Wang, Y., Gu, Y., Liou, K. N., Jiang, J. H., Fan, J., Liu, X., Huang, L., and Yung, Y.
1318 L.: Ice nucleation by aerosols from anthropogenic pollution, *Nat. Geosci.*, 12, 602–607,
1319 <https://doi.org/10.1038/s41561-019-0389-4>, 2019.

1320 Zhu, Z., Peng, C., Li, X., Zhang, R., Dai, X., Jiang, B., and Chen, J.: Remote Sensing Based
1321 Analysis of Precipitation Events: Spatiotemporal Characterization across China, *Water*, 16,
1322 2345, <https://doi.org/10.3390/w16162345>, 2024.